

A three generation oscillation analysis of the Super-Kamiokande atmospheric neutrino data beyond one mass scale dominance approximation

Sandhya Choubey¹, Srubabati Goswami², Kamales Kar³

Saha Institute of Nuclear Physics,

1/AF, Bidhannagar, Calcutta 700064, INDIA.

PACS Numbers: 14.60.Pq, 14.60.Lm, 13.15.+g

keywords: massive neutrino, mixing, atmospheric neutrinos

Abstract

In this paper we do a three-generation oscillation analysis of the latest (1144 days) Super-Kamiokande (SK) atmospheric neutrino data going beyond the one mass scale dominance (OMSD) approximation. We fix $\Delta_{12} = \Delta_{13}$ (Δ_{LSND}) in the range eV^2 as allowed by the results from LSND and other accelerator and reactor experiments on neutrino oscillation and keep Δ_{23} (Δ_{ATM}) and the three mixing angles as free parameters. We incorporate the matter effects, indicate some new allowed regions with small Δ_{23} ($< 10^{-4} \text{ eV}^2$) and $\sin^2 2\theta_{23}$ close to 0 and discuss the differences with the two-generation and OMSD pictures. In our scenario, the oscillation probabilities for the accelerator and reactor neutrinos involve only two of the mixing angles θ_{12} and θ_{13} and one mass scale. But the atmospheric neutrino oscillation is in general governed by both mass scales and all the three mixing angles. The higher mass scale gives rise to Δm^2 independent average oscillations for atmospheric neutrinos and does not enter the χ^2 analysis as an independent parameter. The Δ_{23} and the three mixing angles on the other hand appear as independent parameters in the χ^2 analysis and the best-fit values of these are determined from an analysis of a) the SK data, b) the SK and CHOOZ data. The allowed values of the mixing angles θ_{12} and θ_{13} from the above analysis are compared with the constraints from all accelerator and reactor experiments including the latest results from LSND and KARMEN2. Implications for future long baseline experiments are discussed.

¹sandhya@tnp.saha.ernet.in

²sruba@tnp.saha.ernet.in

³kamales@tnp.saha.ernet.in

1 Introduction

The Super-Kamiokande results on atmospheric neutrino flux measurement show a deficit of the ν_μ flux [1, 2]. Two generation analyses of the SK data show that the $\nu_\mu - \nu_\tau$ oscillation hypothesis provides a very good fit to the SK data [3, 4, 5]⁴. The high statistics of SK also makes it possible to study the zenith-angle dependence of the neutrino flux from which one can conclude that the ν_μ 's show signs of oscillation but the ν_e events are consistent with the no-oscillation hypothesis. Independently the results from the reactor experiment CHOOZ [6] disfavors the $\nu_\mu - \nu_e$ oscillation hypothesis in a two-generation analysis. It is important however to see the implications of these results in a three-generation picture. The most popular three-generation picture in the context of the SK data is the scenario shown in fig. 1a, where one of the mass squared differences is in the solar neutrino range and the other is suitable for atmospheric neutrino oscillations [3, 7]. In such a scheme one mass scale dominance applies for atmospheric neutrinos and the relevant probabilities are functions of two of the mixing angles and one mass squared difference. This picture however cannot explain the LSND results [8]. In this paper we perform a three flavor χ^2 -analysis of the SK atmospheric neutrino data assuming a mass pattern with $\Delta_{12} \simeq \Delta_{13}$ fixed in the eV² range and allowing the other mass scale to vary arbitrarily. This mass pattern is shown in fig. 1b. Apart from being suitable to explain the SK atmospheric neutrino data this spectrum is also interesting for the laboratory based neutrino oscillation experiments as the higher mass scale is explorable in the short base line experiments, whereas the lower mass scale can be probed in the long base line experiments. In this scheme to a good approximation, neutrino oscillation in the short-base line accelerators and reactors will be governed by one (the higher) mass scale [9, 10] – and only two of the mixing angles appear in the expressions for the oscillation probabilities. For the atmospheric and the long baseline experiments the characteristic energy and length scales are such that in general both mass differences are of relevance and the probabilities involve all

⁴The $\nu_\mu - \nu_s$ solution is now ruled out at 99% C.L. by the SK collaboration [2].

the three mixing angles. However the higher mass scale gives rise to Δm^2 independent average oscillations and it does not enter the χ^2 fit directly. We determine the best-fit values of Δ_{23} and the three mixing angles by performing a χ^2 analysis of

- the SK atmospheric neutrino data
- SK atmospheric and CHOOZ data

Finally we compare the allowed values of the mixing angles as obtained from the above analysis with those allowed by the other accelerator and reactor neutrino oscillation data including LSND and KARMEN2.

The mass scheme of this paper was first considered in [11, 12] after the declaration of the LSND result. These papers performed a combined three generation analysis of accelerator and reactor results as well as the Kamiokande atmospheric neutrino data. Three-generation picture with the higher mass difference in the eV^2 range and the lower mass difference in the atmospheric range has also been considered in [13, 14] (pre-SK) and [15, 16, 17, 18] (post-SK). These papers attempted to explain both solar and atmospheric neutrino anomalies mainly by maximal $\nu_\mu \leftrightarrow \nu_e$ oscillations driven by $\Delta_{ATM} \sim 10^{-3} \text{ eV}^2$. Although it was claimed in [15, 16] that this scenario can provide a good fit to all the available data on neutrino oscillations, it was shown in [17] and also later in [18] that this scenario cannot reproduce the zenith angle dependence of the SK atmospheric neutrino data.

In this paper our aim is to determine the allowed oscillation parameter ranges consistent with SK atmospheric, CHOOZ, LSND and other accelerator and reactor experiments. The solar neutrino problem can be explained by invoking a sterile neutrino. We discuss in the conclusions how the solar neutrino flux suppression can be explained in our scenario.

The plan of the paper is as follows. In section 2 we discuss very briefly the atmospheric neutrino code employed for the analysis of the SK data. In section 3 we present the formalism for three-generation oscillation analysis and calculate the required probabilities including the earth matter effects. In section 4 we present the χ^2 analysis of

only SK atmospheric neutrino data. In section 5 we present the combined χ^2 analysis of SK and CHOOZ data. In section 6 we compare the allowed values of mixing angles from the above analyses with those allowed by the other accelerator and reactor data including the latest results from LSND and KARMEN2. In section 7 we discuss the implications of our results for the future long baseline experiments and end in section 8 with some discussions and conclusions.

2 The Atmospheric Neutrino Code

We define the quantities $N_{\mu_{osc}}$ and $N_{e_{osc}}$ as

$$\begin{aligned} N_{\mu_{osc}} &= N_{\mu\mu} + N_{e\mu} \\ N_{e_{osc}} &= N_{ee} + N_{\mu e} \end{aligned}$$

$N_{e,\mu_{osc}}$ are the numbers of e -like and μ -like events in the detector and $N_{ll'}$ is defined as

$$\begin{aligned} N_{ll'} &= n_T \int_0^\infty dE \int_{(E_{l'})_{min}}^{(E_{l'})_{max}} dE_{l'} \int_{-1}^{+1} d \cos \psi \int_{-1}^{+1} d \cos \xi \frac{1}{2\pi} \int_0^{2\pi} d\phi \\ &\times \frac{d^2 F_l(E, \xi)}{dE d \cos \xi} \cdot \frac{d^2 \sigma_{l'}(E, E_{l'}, \cos \psi)}{dE_{l'} d \cos \psi} \epsilon(E_{l'}) \cdot P_{\nu_l \nu_{l'}}(E, \xi). \end{aligned} \quad (1)$$

n_T denotes the number of target nucleons, E is the neutrino energy, $E_{l'}$ is the energy of the final charged lepton, ψ is the angle between the incoming neutrino ν_l and the scattered lepton l' , ξ is the zenith angle of the neutrino and ϕ is the azimuthal angle corresponding to the incident neutrino direction. The zenith angle of the charged lepton is given by

$$\cos \Theta = \cos \xi \cos \psi + \sin \xi \cos \phi \sin \psi \quad (2)$$

$d^2 \sigma_{l'}/dE_{l'} d \cos \psi$ is the differential cross section for $\nu_l N \rightarrow l' X$ scattering, $\epsilon(E_{l'})$ is the detection efficiency for the 1 ring events in the detector and $P_{\nu_l \nu_{l'}}$ is the probability of a neutrino flavour l to convert to a neutrino of flavour l' . We use the atmospheric neutrino fluxes $\frac{d^2 F_l(E, \xi)}{dE d \cos \xi}$ from [19]. For further details regarding the calculation of number of events we refer to [20].

3 Three-Flavor Analysis

3.1 The vacuum oscillation probabilities

The general expression for the probability that an initial ν_α of energy E gets converted to a ν_β after traveling a distance L in vacuum is given by,

$$P(\nu_\alpha, 0; \nu_\beta, t) = \delta_{\alpha\beta} - 4 \sum_{j>i} U_{\alpha i} U_{\beta i} U_{\alpha j} U_{\beta j} \sin^2 \left(\frac{\pi L}{\lambda_{ij}} \right) \quad (3)$$

where λ_{ij} is defined to be the neutrino vacuum oscillation wavelength given by,

$$\lambda_{ij} = (2.47\text{m}) \left(\frac{E}{MeV} \right) \left(\frac{eV^2}{\Delta_{ij}} \right) \quad (4)$$

which denotes the scale over which neutrino oscillation effects can be significant and $\Delta_{ij} = |m_j^2 - m_i^2|$. The actual forms of the various survival and transition probabilities depend on the spectrum of Δm^2 assumed and the choice of the mixing matrix U relating the flavor eigenstates to the mass eigenstates. We choose the flavor states $\alpha = 1, 2$, and 3 to correspond to e, μ and τ respectively. The most suitable parameterization of U for the mass spectrum chosen by us is $U = R_{13}R_{12}R_{23}$ where R_{ij} denotes the rotation matrix in the ij -plane. This yields:

$$U = \begin{pmatrix} c_{12}c_{13} & s_{12}c_{13}c_{23} - s_{13}s_{23} & c_{13}s_{12}s_{23} + s_{13}c_{23} \\ -s_{12} & c_{12}c_{23} & c_{12}s_{23} \\ -s_{13}c_{12} & -s_{13}s_{12}c_{23} - c_{13}s_{23} & -s_{12}s_{13}s_{23} + c_{13}c_{23} \end{pmatrix} \quad (5)$$

where $c_{ij} = \cos \theta_{ij}$ and $s_{ij} = \sin \theta_{ij}$ here and everywhere else in the paper. We have assumed CP-invariance so that U is real. The above choice of U has the advantage that θ_{23} does not appear in the expressions for the probabilities for the laboratory experiments [12].

The probabilities relevant for atmospheric neutrinos are

$$P_{\nu_e \nu_e} = 1 - 2c_{13}^2 c_{12}^2 + 2c_{13}^4 c_{12}^4 - 4(c_{13}s_{12}c_{23} - s_{13}s_{23})^2 (c_{13}s_{12}s_{23} + s_{13}c_{23})^2 S_{23} \quad (6a)$$

$$P_{\nu_\mu \nu_e} = 2c_{13}^2 c_{12}^2 s_{12}^2 - 4c_{12}^2 c_{23} s_{23} (c_{13}s_{12}c_{23} - s_{13}s_{23})(c_{13}s_{12}s_{23} + s_{13}c_{23}) S_{23} \quad (6b)$$

$$P_{\nu_\mu \nu_\mu} = 1 - 2c_{12}^2 s_{12}^2 - 4c_{12}^4 c_{23}^2 s_{23}^2 S_{23} \quad (6c)$$

where $S_{23} = \sin^2(\pi L/\lambda_{23})$. Apart from the most general three generation regime, the following limits are of interest, as we will see later in the context of the SK data:

1. The two-generation limits

Because of the presence of more parameters as compared to the one mass scale dominance picture there are twelve possible two-generation limits [21] with the oscillations driven by either Δ_{LSND} or Δ_{ATM} . Below we list these limits specifying the mass scales that drive the oscillations:

- $s_{12} \rightarrow 0, s_{13} \rightarrow 0$ $(\nu_\mu - \nu_\tau, \Delta_{ATM})$
- $s_{12} \rightarrow 1, s_{13} \rightarrow 0$ $(\nu_e - \nu_\tau, \Delta_{ATM})$
- $s_{12} \rightarrow 0, s_{13} \rightarrow 1$ $(\nu_\mu - \nu_e, \Delta_{ATM})$
- $s_{12} \rightarrow 1, s_{13} \rightarrow 1$ $(\nu_e - \nu_\tau, \Delta_{ATM})$
- $s_{13} \rightarrow 0, s_{23} \rightarrow 0$ $(\nu_\mu - \nu_e, \Delta_{LSND})$
- $s_{13} \rightarrow 0, s_{23} \rightarrow 1$ $(\nu_\mu - \nu_e, \Delta_{LSND})$
- $s_{13} \rightarrow 1, s_{23} \rightarrow 0$ $(\nu_\mu - \nu_\tau, \Delta_{LSND})$
- $s_{13} \rightarrow 1, s_{23} \rightarrow 1$ $(\nu_\mu - \nu_\tau, \Delta_{LSND})$
- $s_{12} \rightarrow 0, s_{23} \rightarrow 0$ $(\nu_e - \nu_\tau, \Delta_{LSND})$
- $s_{12} \rightarrow 0, s_{23} \rightarrow 1$ $(\nu_e - \nu_\tau, \Delta_{LSND})$
- $s_{12} \rightarrow 1, s_{23} \rightarrow 0$ $(\nu_e - \nu_\tau, \Delta_{ATM})$
- $s_{12} \rightarrow 1, s_{23} \rightarrow 1$ $(\nu_e - \nu_\tau, \Delta_{ATM})$

2. $s_{12}^2 = 0.0$

In this limit the relevant probabilities become

$$P_{\nu_e\nu_e} = 1 - 2c_{13}^2s_{13}^2 + 4s_{13}^2c_{23}^2s_{23}^2S_{23} \quad (7a)$$

$$P_{\nu_e\nu_\mu} = 4s_{13}^2s_{23}^2c_{23}^2S_{23} \quad (7b)$$

$$P_{\nu_\mu\nu_\mu} = 1 - 4c_{23}^2s_{23}^2S_{23} \quad (7c)$$

Thus $P_{\nu_\mu\nu_\mu}$ is the same as the two generation limit, $P_{\nu_\mu\nu_e}$ is governed by two of the mixing angles and one mass scale and $P_{\nu_e\nu_e}$ is governed by two mixing angles and both mass scales.

3. $s_{13}^2 = 0.0$

For this case the probabilities take the form

$$P_{\nu_e \nu_e} = 1 - 2c_{12}^2 s_{12}^2 - 4s_{12}^4 c_{23}^2 s_{23}^2 S_{23} \quad (8a)$$

$$P_{\nu_e \nu_\mu} = 2c_{12}^2 s_{12}^2 - 4c_{12}^2 s_{12}^2 c_{23}^2 s_{23}^2 S_{23} \quad (8b)$$

$$P_{\nu_\mu \nu_\mu} = 1 - 2c_{12}^2 s_{12}^2 - 4c_{12}^4 c_{23}^2 s_{23}^2 S_{23} \quad (8c)$$

In this case the probabilities are governed by two mass scales and two mixing angles.

We note that for cases (2) and (3) the probabilities are symmetric under the transformation $\theta_{23} \rightarrow \pi/2 - \theta_{23}$. The probabilities for these cases are functions of at most two mixing angles as in the OMSD case [3] but they are governed by both mass scales making these limits different from the OMSD limit.

3.2 Earth matter effects

Since on their way to the detector the upward going neutrinos pass through the earth, it is important in general to include the matter effect in the atmospheric neutrino analysis. The matter contribution to the effective squared mass of the electron neutrinos:

$$A = 2\sqrt{2} G_F E n_e \quad (9)$$

where E is the neutrino energy and n_e is the ambient electron density. Assuming a typical density of 5 gm/cc and $E = 10$ GeV, the matter potential $A \simeq 3.65 \times 10^{-3}$ eV² and since this is of the same order as Δ_{23} in our case, matter effects should be studied carefully.

The mass matrix in the flavor basis in presence of matter is given by

$$M_F^2 = U M^2 U^\dagger + M_A \quad (10)$$

where M^2 is the mass matrix in the mass eigenbasis, U is the mixing matrix and

$$M_A = \begin{pmatrix} A & 0 & 0 \\ 0 & 0 & 0 \\ 0 & 0 & 0 \end{pmatrix} \quad (11)$$

Since $\Delta_{12} \sim \Delta_{13} \gg \Delta_{23} \sim A$, one can solve the eigenvalue problem using the degenerate perturbation theory, where the Δ_{23} and A terms are treated as a perturbation to the dominant Δ_{12} and Δ_{13} dependent terms. The mixing angle in matter is then given by

$$\tan 2\theta_{23}^M = \frac{\Delta_{23} \sin 2\theta_{23} - A s_{12} \sin 2\theta_{13}}{\Delta_{23} \cos 2\theta_{23} - A(s_{13}^2 - c_{13}^2 s_{12}^2)} \quad (12)$$

while the mass squared difference in matter turns out to be

$$\Delta_{23}^M = \left[(\Delta_{23} \cos 2\theta_{23} - A(s_{13}^2 - c_{13}^2 s_{12}^2))^2 + (\Delta_{23} \sin 2\theta_{23} - A s_{12} \sin 2\theta_{13})^2 \right]^{1/2} \quad (13)$$

The mixing angles θ_{12} and θ_{13} as well as the larger mass squared difference Δ_{12} remain unaltered in matter. From eq. (12) and (13) we note the following

- In the limit of both $s_{12} \rightarrow 0$ and $s_{13} \rightarrow 0$, the matter effect vanishes and we recover the two-generation $\nu_\mu - \nu_\tau$ limit.
- The resonance condition now becomes $\Delta_{23} \cos 2\theta_{23} = A(s_{13}^2 - c_{13}^2 s_{12}^2)$. So that for $\Delta_{23} > 0$, one can have resonance for both neutrinos – if $s_{13}^2 > c_{13}^2 s_{12}^2$ – as well as for antineutrinos – if $s_{13}^2 < c_{13}^2 s_{12}^2$. This is different from the OMSD picture where for $\Delta m^2 > 0$ only neutrinos can resonate [22].
- In the limit of $s_{12} \rightarrow 0$

$$\tan 2\theta_{23}^M = \frac{\Delta_{23} \sin 2\theta_{23}}{\Delta_{23} \cos 2\theta_{23} - A s_{13}^2} \quad (14)$$

Here one gets resonance for neutrinos only (if $\Delta_{23} > 0$) and this is similar to the OMSD case.

- In the limit $s_{13} \rightarrow 0$

$$\tan 2\theta_{23}^M = \frac{\Delta_{23} \sin 2\theta_{23}}{\Delta_{23} \cos 2\theta_{23} + A s_{12}^2} \quad (15)$$

For this case for $\Delta_{23} > 0$, there is no resonance for neutrinos but antineutrinos can resonate.

- In the limit where $\Delta_{23} \rightarrow 0$

$$\tan 2\theta_{23}^M = \frac{s_{12} \sin 2\theta_{13}}{s_{13}^2 - c_{13}^2 s_{12}^2}, \quad \Delta_{23}^M = A(s_{13}^2 + c_{13}^2 s_{12}^2) \quad (16)$$

Thus even for small values of $\Delta_{23} < 10^{-4}$ the mass squared difference in matter is $\sim A$ and one may still hope to see oscillations for the upward neutrinos due to matter effects. The other point to note is that the mixing angle in matter θ_{23}^M depends only on θ_{12} and θ_{13} and is independent of the vacuum mixing angle θ_{23} and Δ_{23} . Contrast this with the OMSD case (where the expressions for $\tan 2\theta_{23}^M$ is given by an expression similar to eq. (14) [22]) and the two-generation $\nu_\mu - \nu_e$ oscillations. For both the two-generation $\nu_\mu - \nu_e$ as well as the three-generation OMSD case, for $\Delta_{23} \rightarrow 0$, the mixing angle $\tan 2\theta_{23}^M \rightarrow 0$, but for the mass spectrum considered in this paper the $\tan 2\theta_{23}^M$ maybe large depending on the values of s_{12}^2 and s_{13}^2 . Hence we see that the *demixing effect* which gives the lower bound on allowed values of Δm^2 in the two generation $\nu_\mu - \nu_e$ or the three-generation OMSD case, does not arise here and we hope to get allowed regions even for very low values of Δ_{23} . On the other hand even small values of θ_{23} in vacuum can get enhanced in matter. This special case where $\Delta_{23} \sim 0$ was considered in an earlier paper [23].

- In the limit of $s_{23}^2 \rightarrow 0$

$$\tan 2\theta_{23}^M = \frac{-As_{12} \sin 2\theta_{13}}{\Delta_{23} - A(s_{13}^2 - c_{13}^2 s_{12}^2)} \quad (17)$$

- While for $s_{23}^2 \rightarrow 1$

$$\tan 2\theta_{23}^M = \frac{-As_{12} \sin 2\theta_{13}}{-\Delta_{23} - A(s_{13}^2 - c_{13}^2 s_{12}^2)} \quad (18)$$

For the last two cases, corresponding to $\sin^2 2\theta_{23} \rightarrow 0$, again the mixing angle θ_{23} in matter is independent of its corresponding value in vacuum and hence for appropriate choices of the other three parameters, Δ_{23} , s_{12}^2 and s_{13}^2 , one can get large values for $\sin^2 2\theta_{23}^M$ even though the vacuum mixing angle is zero.

The amplitude that an initial ν_α of energy E is detected as ν_β after traveling through the earth is

$$A(\nu_\alpha, t_0, \nu_\beta, t) = \sum_{\sigma, \lambda, \rho} \sum_{i, j, k, l} [(U_{\beta l}^{M_m} e^{-iE_l^{M_m}(t-t_3)} U_{\sigma l}^{M_m}) (U_{\sigma k}^{M_m} e^{-iE_k^{M_c}(t_3-t_2)} U_{\lambda k}^{M_c}) \times (U_{\lambda j}^{M_m} e^{-iE_j^{M_m}(t_2-t_1)} U_{\rho j}^{M_m}) (U_{\rho i} e^{-iE_i(t_1-t_0)} U_{\alpha i})] \quad (19)$$

where we have considered the earth to be made of two slabs, a mantle and a core with constant densities of 4.5 gm/cc and 11.5 gm/cc respectively and include the non-adiabatic effects at the boundaries. The mixing matrix in the mantle and the core are given by U^{M_m} and U^{M_c} respectively. $E_i^X \approx m_{iX}^2/2E$, $X = \text{core(mantle)}$ and m_{iX} is the mass of the i^{th} neutrino state in the core(mantle). The neutrino is produced at time t_0 , hits the earth mantle at t_1 , hits the core at t_2 , leaves the core at t_3 and finally hits the detector at time t . The Greek indices (σ, λ, ρ) denote the flavor eigenstates while the Latin indices (i, j, k, l) give the mass eigenstates. The corresponding expression for the probability is given by

$$P(\nu_\alpha, t_0, \nu_\beta, t) = |A(\nu_\alpha, t_0, \nu_\beta, t)|^2 \quad (20)$$

For our calculations of the number of events we have used the full expression given by eq.(19) and (20).

4 χ^2 -analysis of the SK data

We minimize the χ^2 function defined as [3, 4]

$$\chi^2 = \sum_{i, j=1, 40} (N_i^{\text{th}} - N_i^{\text{exp}}) (\sigma_{ij}^{-2}) (N_j^{\text{th}} - N_j^{\text{exp}}) \quad (21)$$

where the sum is over the sub-GeV and multi-GeV electron and muon bins. The experimentally observed number of events are denoted by the superscript ‘‘exp’’ and the theoretical predictions for the quantities are labeled by ‘‘th’’. The element of the error matrix σ_{ij} is calculated as in [3], including the correlations between the different

bins. For contained events there are forty experimental data points. The probabilities for the atmospheric neutrinos are explicit functions of one mass-squared difference and three mixing angles making the number of degrees of freedom (d.o.f) 36. The other mass squared difference gives rise to Δm^2 independent average oscillations and hence does not enter the fit as an independent parameter.

For two-flavour $\nu_\mu - \nu_\tau$ oscillation the 1144 days of data gives the following best-fits and χ_{min}^2 :

- $\chi_{min}^2/d.o.f. = 36.23/38$, $\Delta m^2 = 0.0027 \text{ eV}^2$, $\sin^2 2\theta = 1.0$

This corresponds to a goodness of fit of 55.14%.

For the general three-generation scheme the χ_{min}^2 and the best-fit values of parameters that we get are

- $\chi_{min}^2/d.o.f. = 34.65/36$, $\Delta_{23} = 0.0027 \text{ eV}^2$, $s_{23}^2 = 0.51$, $s_{12}^2 = 0.04$ and $s_{13}^2 = 0.06$

This solution is allowed at 53.28% C.L.

The solid(dashed) lines in fig. 2 present the variation of the $\Delta\chi^2 = \chi^2 - \chi_{min}^2$ for the SK data, with respect to one of the parameters keeping the other three unconstrained, when we include(exclude) the matter effect. In fig. 2(a) as we go towards smaller values of Δ_{23} around 10^{-3} eV^2 the effect of matter starts becoming important as the matter term is now comparable to the mass term. If matter effects are not there then for values of $\Delta_{23} \lesssim 10^{-4} \text{ eV}^2$ the S_{23} term in eq.(6) is very small and there is no up-down asymmetry resulting in very high values of χ^2 as is evident from the dashed curve. If the matter effects are included, then in the limit of very low Δ_{23} the matter term dominates and Δ_{23}^M is given by eq.(16). Since this term $\sim 10^{-3} \text{ eV}^2$ there can be depletion of the neutrinos passing through the earth causing an updown asymmetry. For Δ_{23} around 10^{-4} eV^2 , there is cancellation between the two comparable terms in the numerator of eq. (12) and the mixing angle becomes very small and hence the χ^2 around these values of Δ_{23} comes out to be very high.

Fig 2(b) illustrates the corresponding variation of $\Delta\chi^2$ with s_{23}^2 while the other three parameters are allowed to vary arbitrarily. For small and large values of s_{23}^2

the inclusion of matter effect makes a difference. For s_{23}^2 either very small or large ($\sin^2 2\theta_{23} \rightarrow 0$) the overall suppression of the ν_μ flux is less than that required by the data if vacuum oscillation is operative and so it is ruled out. If we include matter effects then in the limit of $s_{23}^2 = 0$ and $s_{23}^2 = 1$ the matter mixing angle is given by eqs. (17) and (18), which can be large for suitable values of s_{13}^2 and s_{12}^2 and hence one gets lower χ^2 even for these values of s_{23}^2 .

In figs 2(c) and 2(d) we show the effect of s_{12}^2 and s_{13}^2 respectively on $\Delta\chi^2$. From the solid and the dashed lines it is clear that matter effects do not vary much the allowed ranges of s_{12}^2 and s_{13}^2 .

The dashed-dotted line in the figure shows the 99% C.L. (= 13.28 for 4 parameters) limit. In Table 1 we give the allowed ranges of the mixing parameters, inferred from fig. 2 at 99% C.L. for the SK atmospheric data, with and without matter effects.

Table 1: The allowed ranges of parameters for the SK data.

	Δ_{23} in eV ²	s_{23}^2	s_{12}^2	s_{13}^2
with matter effects	$1.6 \times 10^{-4} \leq \Delta_{23} \leq 7.0 \times 10^{-3}$	$0.26 \leq s_{23}^2 \leq 0.77$	$s_{12}^2 \leq 0.21$	$s_{13}^2 \leq 0.55$
	$\Delta_{23} \leq 6.5 \times 10^{-5}$	$s_{23}^2 \geq 0.85$		
without matter effects	$5 \times 10^{-4} \leq \Delta_{23} \leq 7.0 \times 10^{-3}$	$0.27 \leq s_{23}^2 \leq 0.74$	$s_{12}^2 \leq 0.21$	$s_{13}^2 \leq 0.6$

4.1 Zenith-Angle distribution

Since the probabilities in our case are in general governed by two mass scales and all three mixing angles it is difficult to understand the allowed regions. To facilitate the qualitative understanding we present in fig. 3 the histograms which describe the zenith angle distribution. The event distributions in these histograms are approximately given by,

$$\frac{N_\mu}{N_{\mu_0}} \approx P_{\nu_\mu\nu_\mu} + \frac{N_{e_0}}{N_{\mu_0}} P_{\nu_e\nu_\mu} \quad (22)$$

$$\frac{N_e}{N_{e_0}} \approx P_{\nu_e\nu_e} + \frac{N_{\mu_0}}{N_{e_0}} P_{\nu_\mu\nu_e} \quad (23)$$

where the quantities with suffix 0 indicates the no-oscillation values. For the sub-GeV data $N_{\mu 0}/N_{e 0} \approx 2$ to a good approximation however for the multi-GeV data this varies in the range 2 (for $\cos \Theta = 0$) to 3 (for $\cos \Theta = \pm 1$) [3].

In fig. 3a we study the effect of varying s_{12}^2 and s_{13}^2 for fixed values of $\Delta_{23} = 0.002$ eV² and $s_{23}^2 = 0.5$. From eq. (12), (13) and from fig. 2 we see that for the values of the Δ_{23} and s_{23}^2 considered in this figure the matter effects are small and we can understand the histograms from the vacuum oscillation probabilities. The thick solid line shows the event distribution for $s_{12}^2 = 0$ and $s_{13}^2 = 0.1$. As s_{13}^2 increases from 0, keeping s_{12}^2 as 0, from eqs. (9) $P_{\nu_e \nu_e}$ decreases from 1 and $P_{\nu_e \nu_\mu}$ increases from zero resulting in a net electron depletion according to eq. (23). The long dashed line corresponds to $s_{13}^2 = 0.3$ for which the electron depletion is too high as compared to data. The muon events are also affected as $P_{\nu_\mu \nu_e}$ increases with increasing s_{13}^2 even though $P_{\nu_\mu \nu_\mu}$ is independent of s_{13}^2 . On the other hand for $s_{13}^2 = 0.0$, the effect of increasing s_{12}^2 is to increase the number of electron events and decrease the number of muon events according to eqs. (10), (23) and (22). This is shown by the short-dashed and dotted lines in fig. 3a. For $s_{12}^2 = 0.2$ the electron excess and muon depletion both becomes too high as compared to the data. For the case when both s_{12}^2 and s_{13}^2 are 0.1 the electron depletion caused by increasing s_{12}^2 and the excess caused by increasing s_{13}^2 gets balanced and the event distributions are reproduced quite well, shown by the dashed-dotted line.

In fig. 3b we study the effect of varying s_{23}^2 and Δ_{23} in the limit of $s_{12}^2 = 0$ with s_{13}^2 fixed at 0.1. Although we use the full probabilities including the matter effect, for 0.004 eV² this is not so important and one can understand the histograms from the vacuum oscillation probabilities. For fixed Δ_{23} as s_{23}^2 increases, $P_{\nu_\mu \nu_\mu}$ decreases, making the muon depletion higher. This is shown in the figure for two representative values of Δ_{23} . The electron events are not affected much by change of s_{23}^2 . The slight increase with s_{23}^2 is due to increase of both $P_{\nu_e \nu_e}$ and $P_{\nu_\mu \nu_e}$. To understand the dependence on Δ_{23} we note that for $s_{23}^2 = 0.2$, if one looks at the vacuum oscillation probabilities, $N_\mu/N_{\mu 0} \approx 1 - 0.65 S_{23}$. For 0.004 eV² the contribution of S_{23} is more resulting in a lower number of muon events. For the electron events however the behavior with

Δ_{23} is opposite, with $N_e/N_{e0} = 0.82 + 0.12S_{23}$. Thus with increasing Δ_{23} the number of electron events increase. Also note that since the contribution of S_{23} comes with opposite sign the zenith-angle distribution for a fixed Δ_{23} is opposite for the muon and the electron events.

In fig. 3c we show the histograms in the limit of $s_{13}^2 = 0.0$, keeping s_{12}^2 as 0.1 and varying Δ_{23} and s_{23}^2 . As s_{23}^2 increases all the relevant probabilities decrease and therefore both $N_\mu/N_{\mu0}$ and N_e/N_{e0} decrease giving less number of events for both. For this case the S_{23} term comes with the same sign (negative) in both $N_\mu/N_{\mu0}$ and N_e/N_{e0} . Therefore the depletion is more for higher Δ_{23} for both muon and electron events.

Finally, the long dashed line in fig. 3d represent the histograms for the best-fit value for two-generation $\nu_\mu - \nu_\tau$ oscillations, for which $P_{\nu_e\nu_e} = 1$. The short dashed line gives the histograms for the three-generation best-fit values. Both give comparable explanation for the zenith angle distribution of the data. The dotted line gives the event distribution for $\Delta_{23} = 10^{-5} \text{ eV}^2$. As discussed in section 3.2 even for such low value of Δ_{23} , we find that due to the unique feature of the beyond OMSD neutrino mass spectrum, earth matter effects ensure that both the sub-GeV as well as the multi-GeV upward muon events are very well reproduced, as are the electron events. But since s_{12}^2 is high, the downward ν_μ are depleted more than the data requires (eq. (6)).

4.2 Allowed parameter region

In fig. 4a the solid lines give the 99% C.L. allowed area from SK data in the Δ_{23} - s_{23}^2 plane keeping the values of s_{13}^2 and s_{12}^2 fixed in the allowed range from fig. 2 and Table 1. The first panel represents the two-generation $\nu_\mu - \nu_\tau$ oscillation limit modulo the difference in the definition of the C.L. limit as the number of parameters are different. We have seen from the histograms in fig. 3a that raising s_{12}^2 results in electron excess and muon depletion. On the other hand increase in s_{13}^2 causes electron depletion. The above features are reflected in the shrinking and disappearance of the allowed regions in the first row and column. In the panels where both s_{12}^2 and s_{13}^2 are nonzero one may

get allowed regions only when the electron depletion due to increasing s_{13}^2 is replenished by the increase in s_{12}^2 .

In fig. 4b we present the 99% C.L. allowed areas in the bilogarithmic $\tan^2 \theta_{12} - \tan^2 \theta_{13}$ plane for various fixed values of the parameters Δ_{23} and s_{23}^2 . We use the $\log(\tan)$ representation which enlarges the allowed regions at the corners and the clarity is enhanced. The four corners in this plot refer to the two-generation limits discussed in section 3. The extreme left corner ($\theta_{12} \rightarrow 0, \theta_{13} \rightarrow 0$) correspond to the two generation $\nu_\mu - \nu_\tau$ oscillation limit. As we move up increasing θ_{13} , one has $\nu_e - \nu_\mu$ and $\nu_e - \nu_\tau$ mixing in addition and for $s_{13}^2 \rightarrow 1$ one goes to the two generation $\nu_\mu - \nu_e$ oscillation region. For the best-fit values of Δ_{23} and s_{23}^2 if we take s_{12}^2 and s_{13}^2 to be 0 and 1 respectively, then the χ_{min}^2 is 66.92 which is therefore ruled out. Both the right hand corners in all the panels refer to pure $\nu_e - \nu_\tau$ oscillations and therefore there are no allowed regions in these zones. For the panels in the first row, $\Delta_{23} = 0.006 \text{ eV}^2$ and the 2-generation $\nu_\mu - \nu_\tau$ oscillation limit is just disallowed (this can also be seen in the first panel of fig. 4a). The small area allowed for the middle panel of first row (between the solid lines) is due to the fact that for non-zero s_{12}^2 and s_{13}^2 the electron events are better reproduced, while $s_{23}^2 = 0.5$ takes care of the muon events. Hence for this case slight mixture of $\nu_\mu - \nu_e$ and $\nu_e - \nu_\tau$ oscillations is favoured. This feature was also reflected in the fact that in the fig. 4a, the panel for $s_{12}^2 = 0.1$ and $s_{13}^2 = 0.3$ has more allowed range for Δ_{23} than the panel for the 2-generation $\nu_\mu - \nu_\tau$ limit. For the panels with $\Delta_{23} = 0.002 \text{ eV}^2$, both the pure $\nu_\mu - \nu_\tau$ limit as well as full three-generation oscillations, give good fit. For the last two rows with $\Delta_{23} = 0.0007 \text{ eV}^2$ and 0.0004 eV^2 the matter effects are important in controlling the shape of the allowed regions. Infact the allowed region that one gets for 0.0004 eV^2 and $s_{23}^2 = 0.5$ is the hallmark of the matter effect in this particular three-generation scheme. As can be seen from fig. 2a and Table 1, if one does not include the matter effect, then there are no allowed regions below $\Delta_{23} = 0.0005 \text{ eV}^2$ for any arbitrary combination of the other three parameters. Even for the first and the last panels with $\Delta_{23} = 0.0007 \text{ eV}^2$, one gets allowed areas solely due to matter effects.

In fig. 4c the solid lines show the 99% C.L. allowed regions from SK data in the $s_{23}^2 - s_{12}^2$ plane for fixed values of Δ_{23} and s_{13}^2 . In contrast to the previous figure, here (and in the next figure) we use the $\sin - \sin$ representation because the allowed regions are around $\theta_{23} = \pi/4$ and this region gets compressed in the $\log(\tan) - \log(\tan)$ representation. For explaining the various allowed regions we separate the figures in two sets

- For $s_{13}^2 = 0.0$, the four corners of the panels represent the no-oscillation limits inconsistent with the data. Also as discussed in section 3 for $s_{23}^2 = 0.0$ or 1.0 one goes to the limit of pure $\nu_\mu - \nu_e$ conversions driven by Δ_{LSND} , which is not consistent with data. One obtains allowed regions only when s_{23}^2 is close to 0.5 with s_{12}^2 small, so that $\nu_\mu - \nu_\tau$ conversions are dominant. The allowed range of s_{12}^2 is controlled mainly by the electron excess as has been discussed before while the allowed range of s_{23}^2 is determined mostly by the muon depletion.
- For $s_{13}^2 \neq 0$, the four corners represent the two-generation $\nu_e - \nu_\tau$ oscillation limit discussed in section 3 and hence these corners are not allowed. For $s_{23}^2 = 0.0$ or 1.0 and $s_{12}^2 \neq 0$ or 1 one has Δ_{LSND} driven $\nu_\mu - \nu_e$ and $\nu_\mu - \nu_\tau$ conversion and Δ_{ATM} driven $\nu_e - \nu_\tau$ conversions. This scenario is not allowed as it gives excess of electron events and also fails to reproduce the correct zenith angle dependence. For a fixed Δ_{23} as s_{13}^2 increases the electron depletion increases which can be balanced by increasing s_{12}^2 which increases the number of electron events. Hence for a fixed Δ_{23} the allowed regions shift towards higher s_{12}^2 values.

As in fig. 4b the allowed area in the middle panel of the last row is due to the inclusion of the matter effect.

In fig. 4d the solid contours refer to the 99% C.L. allowed areas from SK atmospheric neutrino data in the $s_{13}^2 - s_{23}^2$ plane for various values of Δ_{23} and s_{12}^2 .

- For $s_{12}^2 = 0.0$ the corners represent no oscillation limits. In the limit $s_{23}^2 \rightarrow 0$ or 1 , one gets $\nu_e - \nu_\tau$ oscillation driven by Δ_{LSND} which is also not allowed. For s_{13}^2

$= 0.0$ and $s_{23}^2 \sim 0.5$ one has maximal two-flavour $\nu_\mu - \nu_\tau$ oscillation limit which is therefore allowed (not allowed for $\Delta_{23} = 0.006 \text{ eV}^2$ as discussed before). As s_{13}^2 increases the electron depletion becomes higher and that restricts higher s_{13}^2 values.

- For $s_{12}^2 \neq 0$, the four corners represent two-generation limits driven by Δ_{LSND} . This is the regime of average oscillations and cannot explain the zenith angle dependence of the data. For a fixed Δ_{23} the allowed region first expands and then shrinks in size and also shifts towards higher s_{13}^2 values as s_{12}^2 increases just as in fig. 4c.

Matter effect is important for the last two rows and the increase in the allowed areas for the last two panels of $\Delta_{23} = 0.0004 \text{ eV}^2$ are typical signatures of matter effect.

In fig. 4e we present the allowed range in the $\Delta_{23} - s_{23}^2$ plane with Δ_{23} in the $10^{-5} - 10^{-4} \text{ eV}^2$ range and s_{12}^2, s_{13}^2 fixed at 0.185 and 0.372 respectively. We get allowed regions in this range of small Δ_{23} and small mixing due to matter effects – a feature unique to the mass spectrum considered in this paper.

5 χ^2 analysis of the SK + CHOOZ data

The CHOOZ experiment can probe upto 10^{-3} eV^2 and hence it can be important to cross-check the atmospheric neutrino results. In particular a two-generation analysis shows that CHOOZ data disfavors the $\nu_\mu - \nu_e$ solution to the atmospheric neutrino problem. The general expression for the survival probability of the electron neutrino in presence of three flavours is

$$P_{\nu_e \nu_e} = 1 - 4U_{e1}^2(1 - U_{e1}^2)\sin^2(\pi L/\lambda_{12}) - 4U_{e2}^2U_{e3}^2\sin^2(\pi L/\lambda_{23}) \quad (24)$$

This is the most general expression without the one mass scale dominance approximation. We now minimize the χ^2 defined as

$$\chi^2 = \chi_{ATM}^2 + \chi_{CHOOZ}^2 \quad (25)$$

where we define χ_{CHOOZ}^2 as [5]

$$\chi_{CHOOZ}^2 = \sum_{j=1,15} \left(\frac{x_j - y_j}{\Delta x_j} \right)^2 \quad (26)$$

where x_j are the experimental values, y_j are the corresponding theoretical predictions and the sum is over 15 energy bins of data of the CHOOZ experiment [6]. For the CHOOZ experiment the $\sin^2(\pi L/\lambda_{12})$ term does not always average out to 0.5 (for SK this term always averages to 0.5) and one has to do the energy integration properly. For our analysis we keep the Δ_{12} fixed at 0.5 eV^2 and do a four parameter fit as in SK. The χ_{min}^2 and the best-fit values of parameters that we get are

- $\chi_{min}^2/d.o.f. = 42.22/51$, $\Delta_{23} = 0.0023 \text{ eV}^2$, $s_{23}^2 = 0.5$, $s_{12}^2 = 0.0022$ and $s_{13}^2 = 0.0$.

Thus the best-fit values shift towards the two-generation limit when we include the CHOOZ result. This provides a very good fit to the data being allowed at 80.45% C.L.

The dotted lines in fig. 2 give the combined SK+CHOOZ $\Delta\chi^2 (= \chi^2 - \chi_{min}^2)$ given by eq. (25), as a function of one of the parameters, keeping the other three unconstrained. We find that the CHOOZ data severely restricts the allowed ranges for the parameters s_{12}^2 and s_{13}^2 to values $\lesssim 0.047$, while Δ_{23} and s_{23}^2 are left almost unaffected. Since CHOOZ is consistent with no oscillation one requires $P_{\nu_e\nu_e}$ close to 1. So the second and the third terms in eq. (24) should separately be very small. The second term implies U_{e1}^2 to be close to either 0 or 1. U_{e1}^2 close to zero implies either s_{12}^2 or s_{13}^2 close to 1 which is not consistent with SK. Therefore U_{e1}^2 is close to 1. Then from unitarity both U_{e2}^2 and U_{e3}^2 are close to 0 and so the third term goes to zero irrespective of the value of Δ_{23} and s_{23}^2 . Hence contrary to expectations, CHOOZ puts *almost* no restriction on the allowed values of s_{23}^2 and Δ_{23} , although $\Delta_{23} \sim 10^{-3} \text{ eV}^2$ – in the regime in which CHOOZ is sensitive. On the other hand it puts severe constraints on

the allowed values of s_{12}^2 and s_{13}^2 in order to suppress the average oscillations driven by Δ_{12} . Because of such low values of s_{12}^2 and s_{13}^2 the matter effects for the atmospheric neutrinos are not important and the additional allowed area with low Δ_{23} and high s_{23}^2 obtained in the SK analysis due to matter effects are no longer allowed. The 99% C.L. regions allowed by a combined analysis of SK and CHOOZ data is shown by the dotted lines in figs. 4a-d. It is seen that most of the regions allowed by the three-flavour analysis of the SK data is ruled out when we include the CHOOZ result. None of the allowed regions shown in fig. 4a are allowed excepting the two-generation $\nu_\mu - \nu_\tau$ oscillation limit because CHOOZ does not allow such high values of either s_{13}^2 or s_{12}^2 . Hence we present again in fig. 5 the allowed regions in the $\Delta_{23} - s_{23}^2$ plane for various fixed values of s_{12}^2 and s_{13}^2 , determined from the dotted lines in fig. 2. The solid lines in fig. 5 give the 99% C.L. area allowed by the SK data while the dotted lines give the corresponding allowed region from the combined analysis of SK+CHOOZ. We find that for the combined analysis we get allowed regions in this plane only for much smaller values of s_{12}^2 and s_{13}^2 , which ensures that the electron events are neither less nor more than expectations.

6 Combined allowed area from short baseline accelerator and reactor experiments

As mentioned earlier the higher mass scale of this scenario can be explored in the accelerator based neutrino oscillation search experiments. For the mass-pattern considered the most constraining accelerator experiments are LSND [8], CDHSW [24], E531 [25] and KARMEN [26]. Among these only LSND reported positive evidence of oscillation. Other experiments are consistent with no-oscillation hypothesis. Also important in this mass range are the constraints from the reactor experiment Bugey [27]. The relevant probabilities are [12]

- Bugey

$$P_{\bar{\nu}_e \bar{\nu}_e} = 1 - 4c_{13}^2 c_{12}^2 \sin^2(\pi L/\lambda_{12}) + 4c_{13}^4 c_{12}^4 \sin^2(\pi L/\lambda_{12}) \quad (27)$$

- CDHSW

$$P_{\bar{\nu}_\mu \bar{\nu}_\mu} = 1 - 4c_{12}^2 s_{12}^2 \sin^2(\pi L/\lambda_{12}) \quad (28)$$

- LSND and KARMEN

$$P_{\bar{\nu}_\mu \bar{\nu}_e} = 4c_{12}^2 s_{12}^2 c_{13}^2 \sin^2(\pi L/\lambda_{12}) \quad (29)$$

- E531

$$P_{\nu_\mu \nu_\tau} = 4c_{12}^2 s_{12}^2 s_{13}^2 \sin^2(\pi L/\lambda_{13}) \quad (30)$$

We note that the probabilities are functions of one of the mass scales and two mixing angles. Thus the one mass scale dominance approximation applies. There are many analyses in the literature of the accelerator and reactor data including LSND under this one mass scale dominance assumption [12, 28]. These analyses showed that when one considers the results from the previous (prior to LSND) accelerator and reactor experiments there are three allowed regions in the $\theta_{12} - \theta_{13}$ plane [12, 28]

- low θ_{12} - low θ_{13}
- low θ_{12} - high θ_{13}
- high θ_{12} - θ_{13} unconstrained

When the LSND result was combined with these results then only the first and the third zones remained allowed in the mass range $0.5 \leq \Delta_{12} \leq 2 \text{ eV}^2$. In these earlier analyses of the accelerator and reactor data [12, 28] E776 [29] was more constraining than KARMEN. But with the new data KARMEN2 gives stronger constraint than E776. Also the results from the KARMEN2 experiment now rule out most of the region allowed by the LSND experiment above 1 eV^2 [26]. The LSND collaboration has also now reduced the value of the transition probability that they see [30]. We have

repeated the analysis with the latest LSND and KARMEN results for one representative value of $\Delta_{12} = 0.5 \text{ eV}^2$ and present the allowed region in fig. 6.

The light-shaded area in fig. 6 shows the 90% C.L. allowed area in the bilogarithmic $\tan^2 \theta_{12} - \tan^2 \theta_{13}$ plane from the observance of no-oscillation in all the other above mentioned accelerator and reactor experiments except KARMEN2. The inclusion of the KARMEN2 results as well gives the 90% C.L. region shown by the area shaded by asterix. The 90% allowed region by the LSND experiment is within the dashed lines. The KARMEN2 data severely restricts the LSND allowed regions. The solid line shows the 90% C.L. ($\chi^2 \leq \chi_{min}^2 + 7.78$) region allowed by the combined χ^2 analysis of the SK+CHOOZ data keeping Δ_{23} and s_{23}^2 at 0.002 eV^2 and 0.5 respectively. The combined SK atmospheric and the CHOOZ reactor data rule out the third zone (high θ_{12} with θ_{13} unconstrained) allowed from LSND and other accelerator and reactor experiments. Thus if one takes into account constraints from all experiments only a small region in the first zone (small θ_{12}, θ_{13}) remains allowed. This common allowed region is shown as a dark-shaded area in the fig. 6. As evident from the expression of the probabilities for the accelerator and reactor experiments the combined allowed area of all the accelerator reactor experiments remains the same irrespective of the value of Δ_{23} and s_{23}^2 . Even though the combined area in fig. 6 shows that in the first zone (small θ_{12}, θ_{13}), SK+CHOOZ data allows more area in the $\theta_{12} - \theta_{13}$ plane for $\Delta_{23} = 0.002 \text{ eV}^2$ and $s_{23}^2 = 0.5$, from fig. 4b we see that for some other combinations of Δ_{23} and s_{23}^2 one does not find any allowed zones from the SK+CHOOZ analysis, even at 99% C.L.. For those sets of values of Δ_{23} and s_{23}^2 the SK+CHOOZ analysis is more restrictive than the LSND and other accelerator reactor data.

7 Implications

From our analysis of the SK atmospheric data the explicit form for the 3×3 mixing matrix U at the best-fit values of parameters is

$$U = \begin{pmatrix} 0.95 & -0.039 & 0.31 \\ -0.2 & 0.686 & 0.7 \\ -0.24 & -0.727 & 0.644 \end{pmatrix} \quad (31)$$

From the combined SK+CHOOZ analysis the mixing matrix at the best-fit values of the parameters is

$$U = \begin{pmatrix} 0.999 & 0.033 & 0.033 \\ -0.047 & 0.706 & 0.706 \\ -0.0 & -0.707 & 0.707 \end{pmatrix} \quad (32)$$

From the combined allowed area of fig. 6 the mixing matrix at $\Delta_{12} = 0.5 \text{ eV}^2$, $\Delta_{23} = 0.0028 \text{ eV}^2$, $s_{12}^2 = 0.005$, $s_{13}^2 = 0.001$ and $s_{23}^2 = 0.5$, is

$$U = \begin{pmatrix} 0.997 & 0.028 & 0.072 \\ -0.071 & 0.705 & 0.705 \\ -0.032 & -0.708 & 0.705 \end{pmatrix} \quad (33)$$

Thus the allowed scenario corresponds to the one where $\langle \nu_1 | \nu_e \rangle$ is close to 1 while the states ν_2 and ν_3 are combinations of nearly maximally mixed ν_μ and ν_τ ⁵.

Long baseline (LBL) experiments can be useful to confirm if the atmospheric neutrino anomaly is indeed due to neutrino oscillations, using well monitored accelerator neutrino beams. Some of the important LBL experiments are K2K⁶ (KEK to SK, $L \approx 250 \text{ km}$)[31], MINOS (Fermilab to Soudan, $L \approx 730 \text{ km}$) [32] and the proposed CERN to Gran Sasso experiments ($L \approx 730 \text{ km}$) [33]. In this section we explore the sensitivity of the LBL experiment K2K in probing the parameter spaces allowed by the SK+CHOOZ and other accelerator and reactor experiments including LSND. K2K will look for ν_μ disappearance as well as ν_e appearance. In fig. 7 we show the regions in the $\Delta_{23} - s_{23}^2$ plane that can be probed by K2K using their projected sensitivity from [31]. The top left panel is for the two-generation $\nu_\mu - \nu_\tau$ limit. The other panels are for

⁵ Thus this scenario is the same as the one termed 3a in Table VI in the pre-SK analysis of [14]. In their notation the states 2 and 3 were 1 and 2. It was disfavoured from solar neutrino results.

⁶K2K has already presented some preliminary results.

different fixed values of s_{12}^2 and s_{13}^2 while Δ_{12} is fixed at 0.5 eV^2 . For LBL experiments the term containing Δ_{12} averages to 0.5 as in the atmospheric case. The solid lines in the panels show the region that can be probed by K2K using the ν_μ disappearance channel while the dotted lines give the 90% C.L. contours allowed by SK+CHOOZ. One finds that for $\Delta_{23} \geq 2 \times 10^{-3} \text{ eV}^2$, the whole region allowed by SK+CHOOZ can be probed by the ν_μ disappearance channel in K2K. The dashed lines show the 90% C.L. area that K2K can probe by the ν_e appearance mode. As s_{12}^2 increases the constraint from the $P_{\nu_\mu\nu_e}$ channel becomes important as is seen in the top right panel of fig. 7. However such high values of s_{12}^2 , although allowed by SK+CHOOZ, is not favoured when one combines LSND and other accelerator and reactor results. For lower s_{12}^2 values allowed by all the accelerator, reactor and SK atmospheric neutrino experiment the projected sensitivity in the $\nu_\mu - \nu_e$ channel of K2K is not enough to probe the allowed regions in the $\Delta_{23} - s_{23}^2$ plane as is shown by the absence of the dashed curves in the lower panels.

In fig. 8 we show the regions in the bilogarithmic $\tan^2 \theta_{12} - \tan^2 \theta_{13}$ plane which can be probed by K2K. For drawing these curves we fix $\Delta_{23} = 0.002 \text{ eV}^2$, $s_{23}^2 = 0.5$ and $\Delta_{12} = 0.5 \text{ eV}^2$. Shown is the area that can be explored by the $\nu_\mu - \nu_\mu$ (left of the solid line) and $\nu_\mu - \nu_e$ (hatched area) channels in K2K at 90% C.L.. The light-shaded area is allowed by SK+CHOOZ and the dark shaded area is allowed by the combination of all the accelerator, reactor and SK atmospheric neutrino data at 90% C.L.. It is clear from the figure that even though the sensitivity of the ν_e appearance channel is not enough, K2K can still probe the combined allowed region in the $\theta_{12} - \theta_{13}$ plane from ν_μ disappearance.

The projected sensitivities of MINOS and the CERN to ICARUS proposals are lower than K2K and it will be interesting to check if one can probe the regions allowed in this picture better in these experiments. However since in our case the OMSD approximation is not applicable one has to do the energy averaging properly to get the corresponding contours in the three-generation parameters space, and one cannot merely scale the allowed regions from the two-generation plots. For K2K we could use

the fig. 5 of [31] to circumvent this problem. However since the analogous information for MINOS and CERN-Gran Sasso proposals is not available to us we cannot check this explicitly.

An important question in this context is whether one can distinguish between the OMSD three generation and this mass scheme. In both pictures the SK atmospheric neutrino data can be explained by the dominant $\nu_\mu - \nu_\tau$ oscillations mixed with little amount of $\nu_e - \nu_\mu(\nu_\tau)$ transition. However the mixing matrix U is different. A distinction can be done if one can measure the mixing angles very accurately.

What is the prospect in LBL experiments to distinguish between these pictures? We give below a very preliminary and qualitative discussion on this. If we take $s_{12}^2 = 0.02$, $s_{13}^2 = 0.02$ and $s_{23}^2 = 0.5$, $P_{\nu_\mu\nu_e}$ would be $(0.038 + 0.0004 \langle S_{23} \rangle)$. As the second term is negligible one has average oscillations. This is different from the OMSD limit where $P_{\nu_\mu\nu_e} = 4U_{\mu 3}^2 U_{e 3}^2 S_{23}$ is energy dependent. If one combines the other accelerator and reactor experiments including LSND then the allowed values of s_{12}^2 and s_{13}^2 are even less and choosing $s_{12}^2 = 0.005$, $s_{13}^2 = 0.001$ and $s_{23}^2 = 0.5$ we get $P_{\nu_e\nu_\mu} = 0.01 - 0.004 \langle S_{23} \rangle$. Here also the term involving $\langle S_{23} \rangle$ is one order of magnitude smaller and the oscillations will be averaged. Thus this channel has different predictions for the OMSD limit and beyond the OMSD limit.

8 Discussions and Conclusions

In this paper we have done a detailed χ^2 analysis of the SK atmospheric neutrino data going beyond the OMSD approximation. The mass spectrum chosen is such that $\Delta_{12} = \Delta_{13} \sim \text{eV}^2$ to explain the LSND data and Δ_{23} is in the range suitable for the atmospheric neutrino problem. We study in details the implications of the earth matter effects and bring out the essential differences of our mass pattern with the OMSD scenario and the two-generation limits.

We first examine in detail what are the constraints obtained from only SK data considering its overwhelming statistics. The allowed regions include

- the two-generation $\nu_\mu - \nu_\tau$ limit (both s_{12}^2 and s_{13}^2 zero)
- regions where either s_{12}^2 or s_{13}^2 is zero; in this limit the probabilities are functions in general of two mixing angles and two mass scales.
- the three-generation regions with all three mixing angles non-zero and the probabilities governed by both mass scales.

The last two cases correspond to dominant $\nu_\mu - \nu_\tau$ oscillation with small admixture of $\nu_\mu - \nu_e$ and $\nu_e - \nu_\tau$ oscillation.

- regions with very low Δ_{23} ($< 10^{-4}$ eV²) and s_{23}^2 close to 1, for which the earth matter effects enhance the oscillations of the upward neutrinos and cause an up-down flux asymmetry. This region is peculiar to the mass spectrum considered by us and is absent in the two-generation and the OMSD pictures.

We present the zenith angle distributions of the events in these cases. With the inclusion of the CHOOZ result the allowed ranges of the mixing angles s_{12}^2 and s_{13}^2 is constrained more ($\lesssim 0.047$), however the allowed ranges of Δ_{23} and s_{23}^2 do not change much (see fig. 2) except that the low Δ_{23} region allowed by SK due to matter effects is now disallowed. The inclusion of the constraints from LSND and other accelerator and reactor experiments may restrict the allowed area in the $\theta_{12} - \theta_{13}$ plane for certain values of Δ_{23} and s_{23}^2 , but for some other combinations of Δ_{23} and s_{23}^2 , SK+CHOOZ turns out to be more constraining. We have included the latest results from LSND and KARMEN2 in our analysis.

In order to explain the solar neutrino problem in this picture one has to add an extra light sterile neutrino. With the new LSND results the allowed 4 neutrino scenarios are

- the (2+2) picture where two degenerate mass states are separated by the LSND gap [21, 34, 35, 36].
- the (3+1) scheme with three neutrino states closely degenerate in mass and the fourth one separated from these by the LSND gap [36, 37]. In [36] the separated

state is predominantly a sterile state. In [37], on the other hand, the state separated by the LSND gap has a very small sterile component.

The extension of our scenario to the 2+2 picture is straight forward. One has to add an extra sterile state 4 close to the state 1 such that Δ_{14} is in the solar range. Then we have two almost decoupled two-generation pictures in which the atmospheric neutrino problem is mainly due to $\nu_\mu - \nu_\tau$ oscillation and the solar neutrino problem is explained by $\nu_e - \nu_s$ oscillation. The SMA MSW solution for two -generation $\nu_e - \nu_s$ picture is allowed at $\sim 15\%$ C.L. [38]. A detailed global fit of solar and atmospheric neutrino data under this picture would tell us how much this will change due to the small admixture with the other generations. If on the other hand we assume the 4th state to be close to the 2nd and the third state then we will have a (3+1) picture where the 1 state, separated by the LSND gap, is predominantly ν_e . This picture will have difficulties in solving the solar neutrino problem as because of the CHOOZ constraints U_{ei} ($i=2,3,4$) are small so that $P_{\nu_e\nu_e} \approx 1$ indicating very small suppression of the solar neutrino flux.

To conclude, one can get allowed regions from the SK atmospheric neutrino data where both the mass scales and all the three mixing angles are relevant. The beyond one mass scale dominance spectrum considered in this paper allows new regions in the low mass – low mixing regime due to the earth matter effects. With the inclusion of the CHOOZ, LSND and other accelerator reactor results, the allowed regions are constrained severely. It is, in principle, possible to get some signatures in the LBL experiments to distinguish this picture from the OMSD limit.

The authors wish to thank Kenji Kaneyuki for sending them the 1144 days SK atmospheric data and the detection efficiencies. They also wish to thank E. Lisi, N. Fornengo and S. Uma Sankar for useful correspondences.

References

- [1] Y. Fukuda *et al.*, The Super-Kamiokande Collaboration, Phys. Lett. **B433**, 9 (1998); Phys. Lett. **B436**, 33 (1998); Phys. Rev. Lett. **81**, 1562 (1998).
- [2] S. Fukuda *et al.*, The Super-Kamiokande Collaboration, hep-ex/0009001.
- [3] G.L. Fogli, E. Lisi, A. Morroni, G. Scioscia, Phys. Rev. **D59**, 033001 (1998).
- [4] M.C. Gonzalez-Garcia, H. Nunokawa, O.L.G. Peres, T. Stanev, J.W.F. Valle, Phys. Rev. **D58**, 033004 (1998); M.C. Gonzalez-Garcia, H. Nunokawa, O.L.G. Peres, J.W.F. Valle, Nucl. Phys. **B543**, 3 (1999); N. Fornengo, M.C. Gonzalez-Garcia, J.W.F. Valle, Nucl. Phys. **B580**, 58 (2000).
- [5] R. Foot, R.R. Volkas and O. Yasuda, Phys. Rev. **D58** 013006, (1998) .
- [6] M. Apollonio *et al.*, Phys. Lett. **B 420**, 397 (1998); Phys. Lett. **B 466**, 415 (1999).
- [7] O. Yasuda, Phys. Rev.**D 58**,091301, (1998); hep-ph/9809205, to be published in the proceedings of Symposium on new era in neutrino physics, Tokyo, Japan, 11-12 June, 1998.
- [8] C. Athanassopoulos *et al.*, Phys. Rev. Lett. **75**, 2650 (1995); C. Athanassopoulos *et al.*, Phys. Rev. Lett. **81**, 1774 (1998); Talk presented by the LSND Collaboration in *Neutrino 2000*, Sudbury, Canada, 2000.
- [9] V. Barger, *et al.*, Phys. Lett. **B93**, 195 (1980); J. Phys. G **6**, L165 (1980); V. Barger, K. Whisnant and R.J.N. Phillips, Phys. Rev **D22**, 1636 (1980); A. De Rújula *et al.*, Nucl. Phys. **B168**, 54 (1980).
- [10] G.L. Fogli, E. Lisi and D. Montanio, Phys. Rev. **D49**, 3626 (1994).
- [11] H. Minakata, Phys. Rev. **D52**, 6630 (1995).
- [12] S. Goswami, K. Kar and A. Raychaudhuri, hep-ph/9505395, Int. J. Mod. Phys. **A12**, 781 (1997).
- [13] A. Acker and S. Pakvasa, Phys. Lett. **B397**, 209 (1997).

- [14] G.L. Fogli, E. Lisi, D. Montanino and G. Scioscia, Phys. Rev. **D56**, 4365 (1997).
- [15] R.P. Thun and S. McKee, Phys. Lett. **B439**, 123 (1998); G. Marengo and F. Scheck, *ibid* **B440**, 332 (1998); G. Conforto, M. Barone and C. Grimani, *ibid* **B447**, 122 (1999).
- [16] T. Ohlsson and H. Snellman, Phys. Rev. **D60**, 093007 (1999).
- [17] G.L. Fogli, E. Lisi, A. Marrone and G. Scioscia, hep-ph/9906450.
- [18] C. Meier, T. Ohlsson, hep-ph/9910270.
- [19] M. Honda, T. Kajita, S. Midorikawa, and K. Kasahara, Phys. Rev. **D52**, 4985 (1995).
- [20] S. Choubey and S. Goswami, Astropart. Phys. **14**, 67 (2000).
- [21] S. Goswami, Phys. Rev. **D55**, 2931 (1997)
- [22] M. Narayan *et al.*, Phys. Rev. **D** (1996).
- [23] A. De. Rujula, M.B. Gavela and P. Hernandez, hep-ph/0001124.
- [24] F. Dydak *et al.*, Phys. Lett. **B314**, 281 (1984).
- [25] N. Ushida *et al.*, Phys. Rev. Lett. **57**, 2898 (1986).
- [26] Talk presented by KARMEN Collaboration, at *Neutrino 2000*, Sudbury, Canada, 2000.
- [27] B. Achkar *et al.*, Nucl. Phys. **B434**, 503 (1995).
- [28] G.L. Fogli, E. Lisi and G. Scioscia, Phys. Rev. **D52**, 5334 (1995).
- [29] L. Borodovsky *et al.*, Phys. Rev. Lett. **68**, 274 (1992).
- [30] Last one of [8].

- [31] Y. Oyama, hep-ex/9803014.
- [32] MINOS Collaboration, "Neutrino Oscillation Physics at Fermilab": The NuMI-MINOS Project," Report NuML-L-375 (1998),
http://www.hep.anl.gov/ndk/hypertext/numi_notes.html.
- [33] C. Acquistapace *et al.*, "The CERN Neutrino beam to Gran Sasso (NGS), INFN/AE-98/05 (1998).
- [34] S.M. Bilenky, C.Giunti, W.Grimus, Phys. Rev. **D57**, 1920 (1998); Phys. Rev. **D58**, 033001 (1998).
- [35] J.J. Gomez-Cadenas and M.C. Gonzalez-Garcia, Zeit. Phys. **C71**, 443 (1996); N. Okada and O. Yasuda, Int. J. Mod. Phys. **A12**, 3669 (1997).
- [36] B. Barger *et al.* Phys. Lett. **B489**, 345, (2000).
- [37] C. Giunti and Marco Laveder, hep-ph/0010009.
- [38] A. Bandyopadhyay, S. Choubey and S. Goswami, hep-ph/0101273, to appear in Physical Review D.

Figure Captions

Fig. 1: The two possible neutrino mass spectra in a three generation scheme.

Fig. 2: The variation of $\Delta\chi^2 = \chi^2 - \chi_{min}^2$ with one of the parameters keeping the other three unconstrained. The solid (dashed) line corresponds to only SK data when matter effects are included (excluded) while the dotted curve gives the same for SK+CHOOZ. The dashed-dotted line shows the 99% C.L. limit for 4 parameters.

Fig. 3a: The zenith angle distribution of the lepton events with $\Delta_{23} = 0.002 \text{ eV}^2$ and $s_{23}^2 = 0.5$ for various combinations of s_{12}^2 and s_{13}^2 . N is the number of events as given by eq. (1) and N_0 is the corresponding number with survival probability 1. The panels labelled SG_α and MG_α (α can be e or μ) give the histograms for the sub-GeV and multi-GeV α -events respectively. Also shown are the SK experimental data points with $\pm 1\sigma$ error bars.

Fig. 3b: Same as in fig. 3a for fixed $s_{12}^2 = 0.1$ and $s_{13}^2 = 0.0$ varying Δ_{23} and s_{23}^2 .

Fig. 3c: Same as in fig. 3a fixing $s_{12}^2 = 0.0$ and $s_{13}^2 = 0.1$ for different Δ_{23} and s_{23}^2 values.

Fig. 3d: The long-dashed (short-dashed) line gives the zenith angle distribution of the lepton events for the best-fit cases of the two-generation (three-generation) oscillation solutions for SK. The dotted line gives the corresponding distribution for $\Delta_{23} = 10^{-5} \text{ eV}^2$, $s_{12}^2 = 0.2$, $s_{13}^2 = 0.4$ and $s_{23}^2 = 1.0$.

Fig. 4a: The allowed parameter regions in the $\Delta_{23} - s_{23}^2$ plane for various fixed values of s_{12}^2 and s_{13}^2 , shown at the top of each panel. The solid lines corresponds to the 99% C.L. contours from the SK data alone, while the dotted line gives the 99% contour from the combined analysis of the SK+CHOOZ data.

Fig. 4b: Same as 4a but in the bilogarithmic $\tan^2 \theta_{12} - \tan^2 \theta_{13}$ plane for fixed values of Δ_{23} and s_{23}^2 .

Fig. 4c: Same as 4a but in the $s_{12}^2 - s_{23}^2$ plane for fixed values of s_{13}^2 and Δ_{23} .

Fig. 4d: Same as 4a but in the $s_{13}^2 - s_{23}^2$ plane for various fixed values of s_{12}^2 and Δ_{23} .

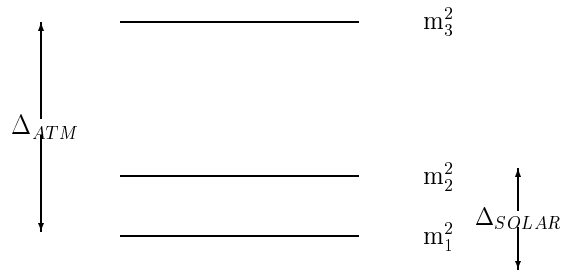
Fig. 4e: The allowed parameter space in the $\Delta_{23} - s_{23}^2$ plane with Δ_{23} in the range $10^{-5} - 10^{-4} \text{ eV}^2$ and with fixed values of $s_{12}^2 = 0.185$ and $s_{13}^2 = 0.372$.

Fig. 5: Same as 4a but for smaller values of s_{12}^2 and s_{13}^2 , chosen from the range determined by the SK+CHOOZ dashed line in fig. 3.

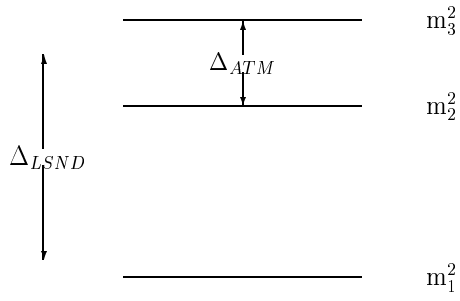
Fig. 6: The area between the dashed lines is the 90% C.L. region allowed by LSND while the light shaded zone gives the 90% C.L. allowed region from the non-observance of neutrino oscillation in the other short baseline accelerator and reactor experiments except KARMEN2. The corresponding area which includes KARMEN2 as well is shown by the region shaded by asterix. The 90% C.L. allowed region from SK+CHOOZ analysis is within the dotted line. The dark shaded area corresponds to the combined allowed region.

Fig. 7: 90% C.L. regions in the $\Delta_{23} - s_{23}^2$ plane that can be explored by the $\nu_\mu - \nu_\mu$ (solid line) and $\nu_\mu - \nu_e$ (dashed line) oscillation channels in the K2K experiment. The area inside the dotted line shows the 90% C.L. region allowed by SK+CHOOZ. The curves are presented for fixed values of s_{12}^2 and s_{13}^2 with $\Delta_{12} = 0.5 \text{ eV}^2$.

Fig. 8: Sensitivity of the K2K experiment in the $\tan^2 \theta_{12} - \tan^2 \theta_{13}$ plane for $\Delta_{23} = 0.002 \text{ eV}^2$, $s_{23}^2 = 0.5$ and $\Delta_{12} = 0.5 \text{ eV}^2$. The area that can be explored by the $\nu_\mu - \nu_\mu$ (left of solid line) and $\nu_\mu - \nu_e$ (hatched area) channels in K2K at 90% C.L. is shown. The light-shaded area is allowed by SK+CHOOZ and the dark-shaded region is the combined area allowed by all accelerator and reactor data at 90% C.L..



(a)



(b)

Fig. 1

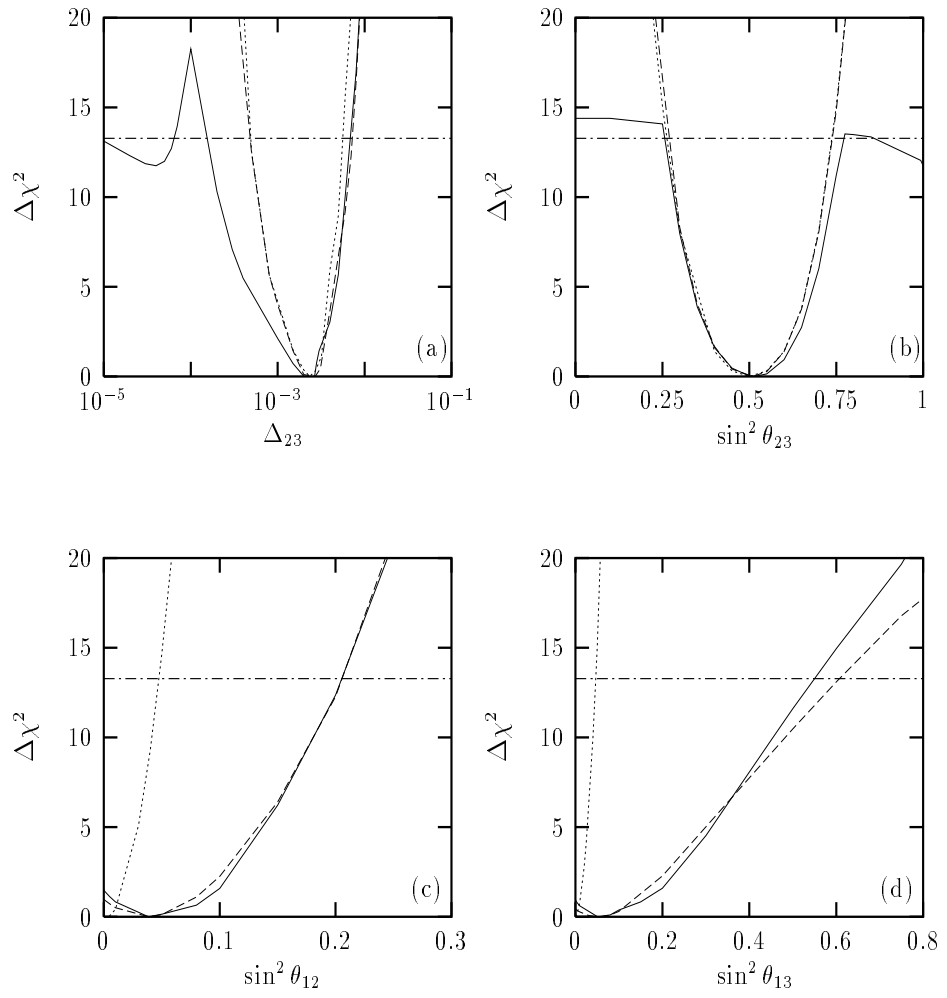
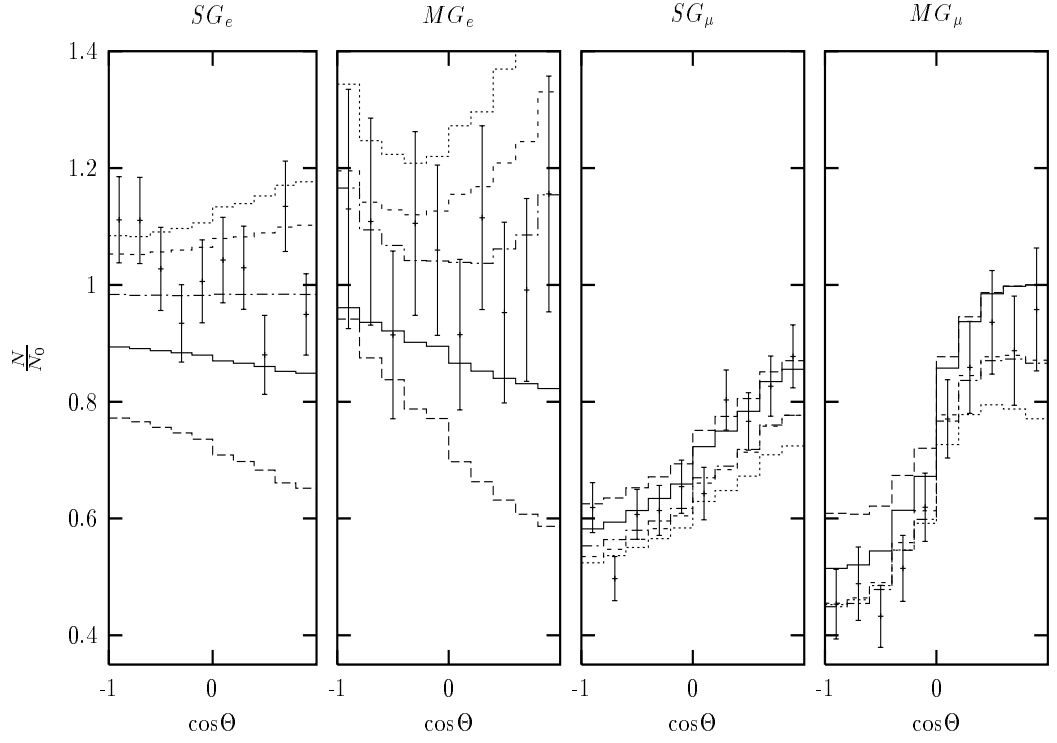
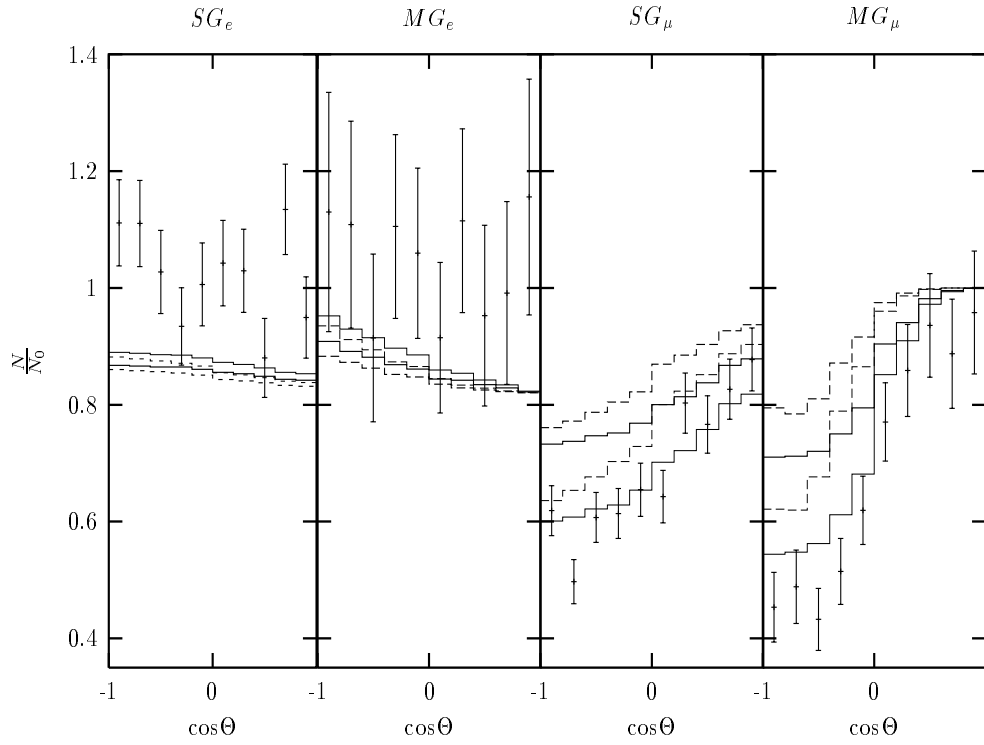


Fig. 2



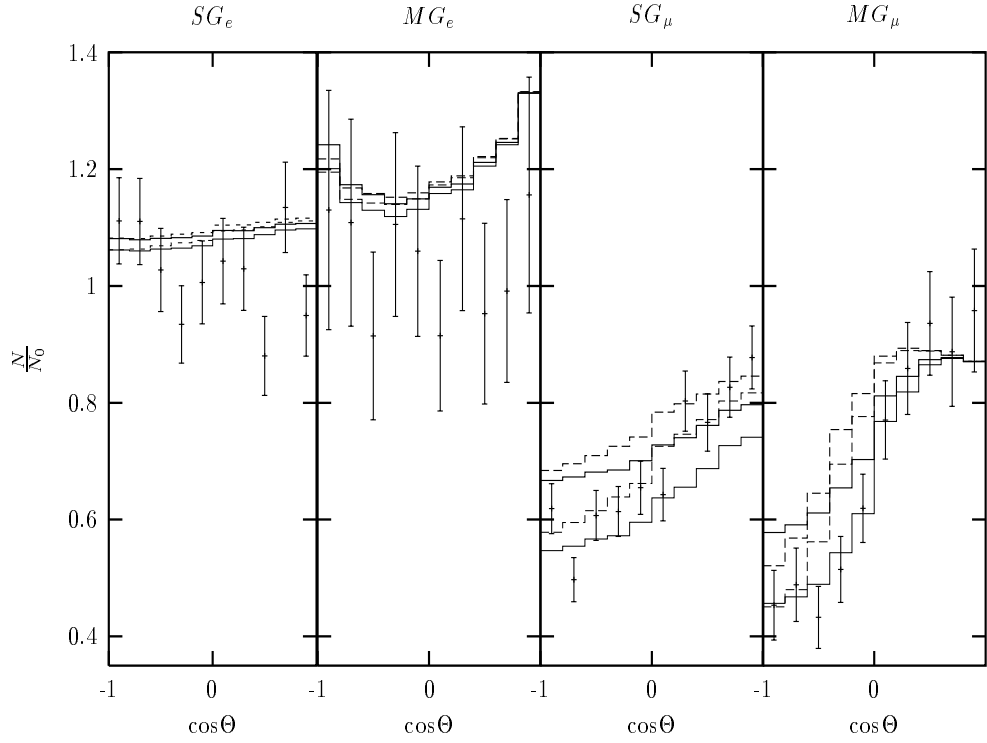
line type	Δ_{23}	s_{23}^2	s_{12}^2	s_{13}^2
thick solid	0.002 eV^2	0.5	0.0	0.1
long dashed	0.002 eV^2	0.5	0.0	0.3
short dashed	0.002 eV^2	0.5	0.1	0.0
dotted	0.002 eV^2	0.5	0.2	0.0
dashed-dotted	0.002 eV^2	0.5	0.1	0.1

Fig. 3a



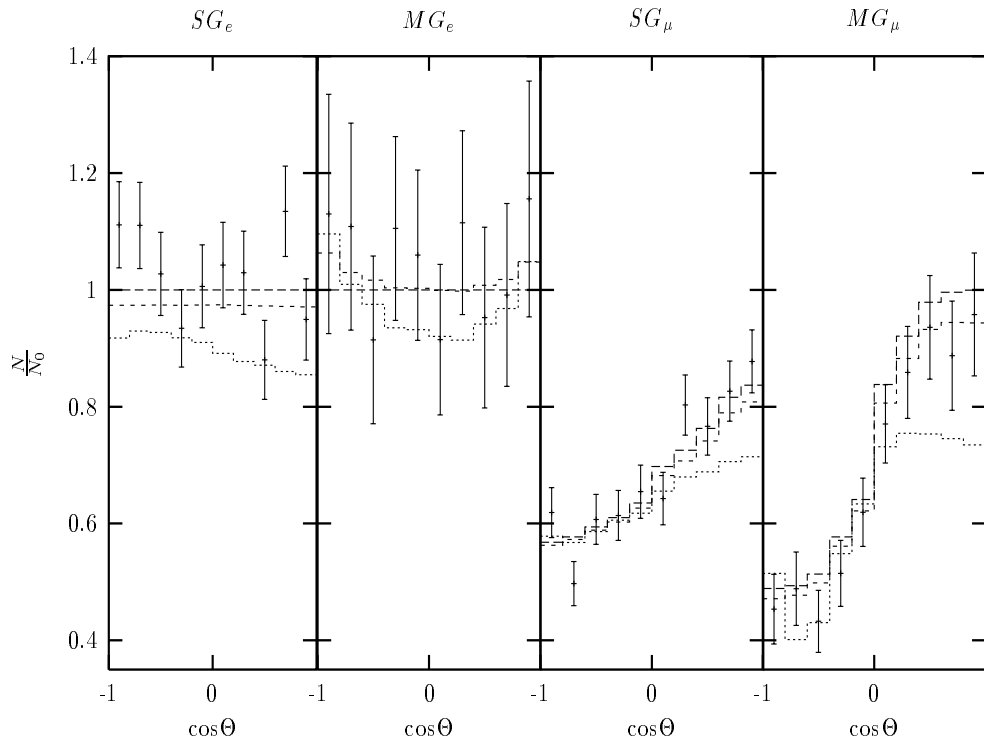
line type	Δ_{23}	s_{23}^2	s_{12}^2	s_{13}^2
thick solid	0.004 eV ²	0.2	0.0	0.1
thick dashed	0.0004 eV ²	0.2	0.0	0.1
thin solid	0.004 eV ²	0.4	0.0	0.1
thin dashed	0.0004 eV ²	0.4	0.0	0.1

Fig. 3b



line type	Δ_{23}	s_{23}^2	s_{12}^2	s_{13}^2
thick solid	0.004 eV^2	0.2	0.1	0.0
thick dashed	0.0004 eV^2	0.2	0.1	0.0
thin solid	0.004 eV^2	0.4	0.1	0.0
thin dashed	0.0004 eV^2	0.4	0.1	0.0

Fig. 3c



line type	Δ_{23}	s_{23}^2	s_{12}^2	s_{13}^2
long dashed	0.0027 eV^2	0.5	0.0	0.0
short dashed	0.0027 eV^2	0.51	0.04	0.06
dotted	0.00001 eV^2	1.0	0.2	0.4

Fig. 3d

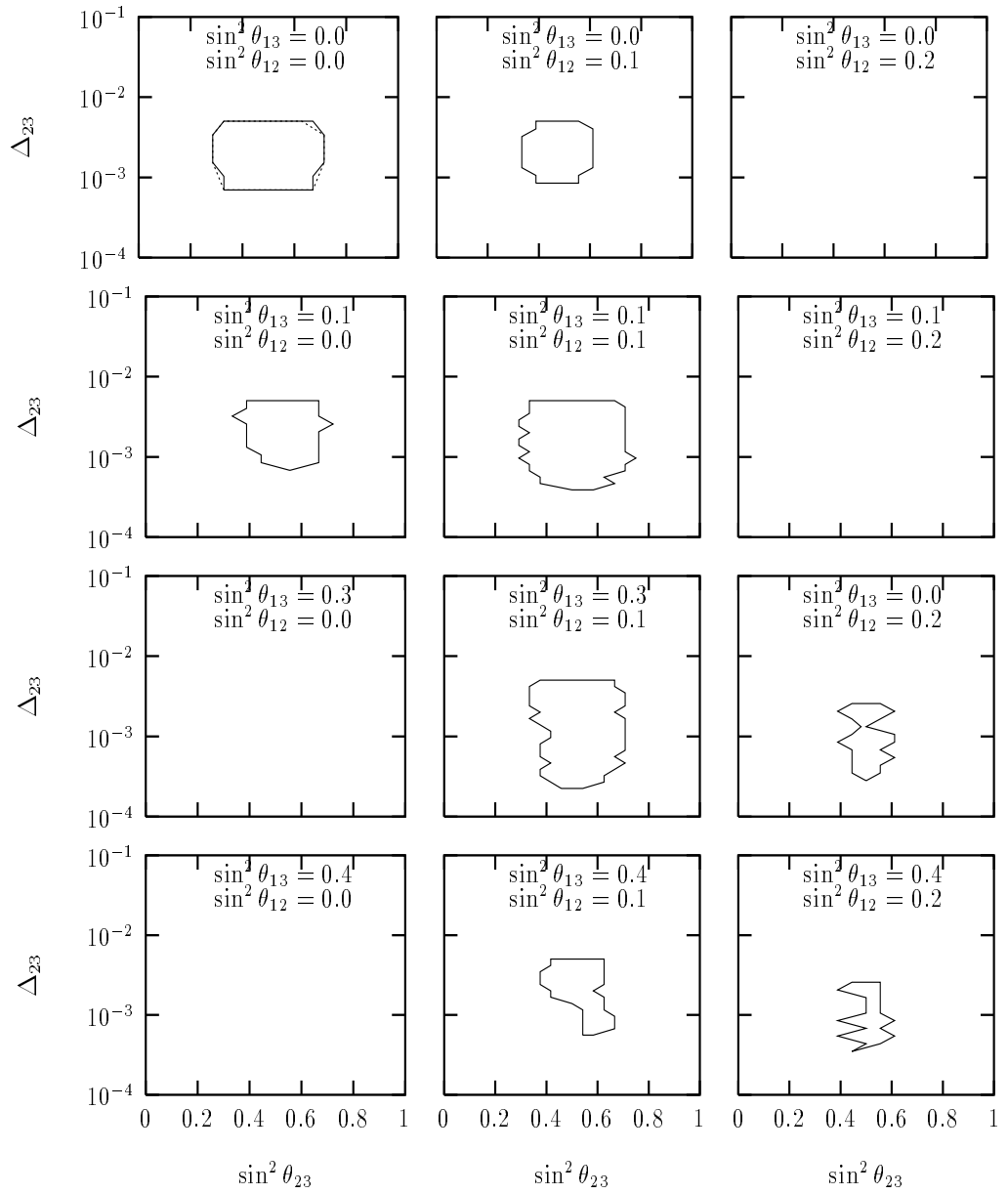


Fig. 4a

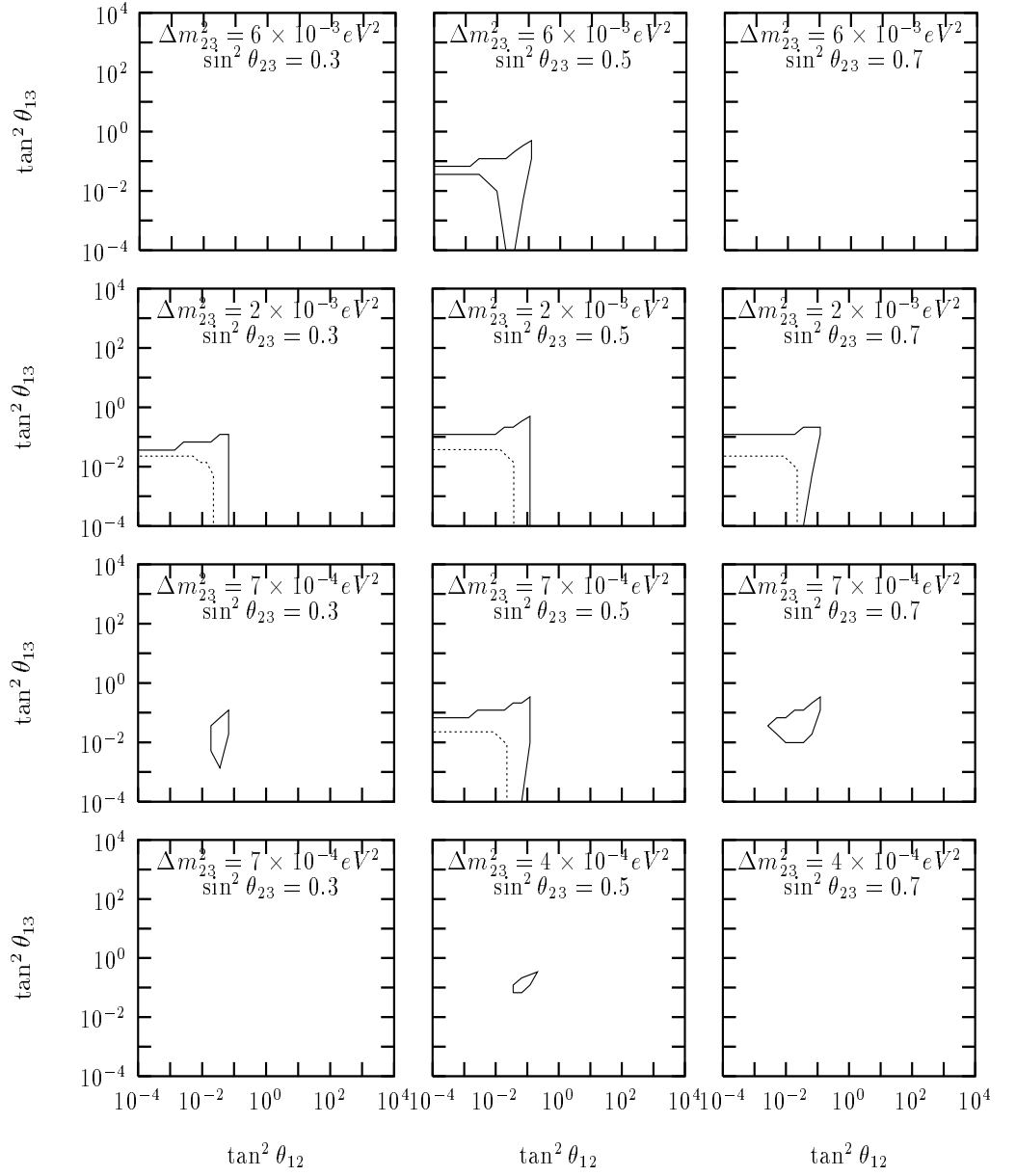


Fig. 4b

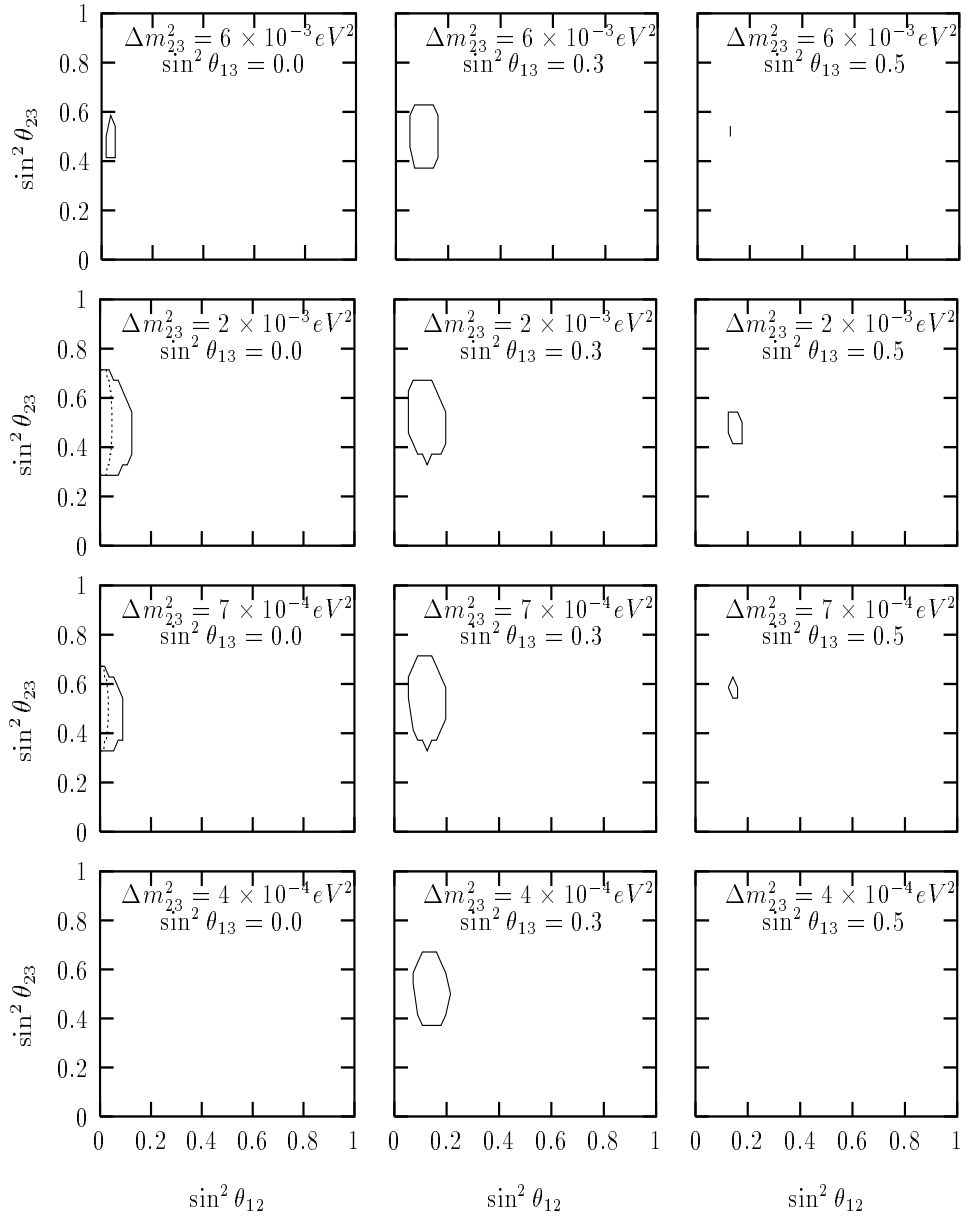


Fig. 4c

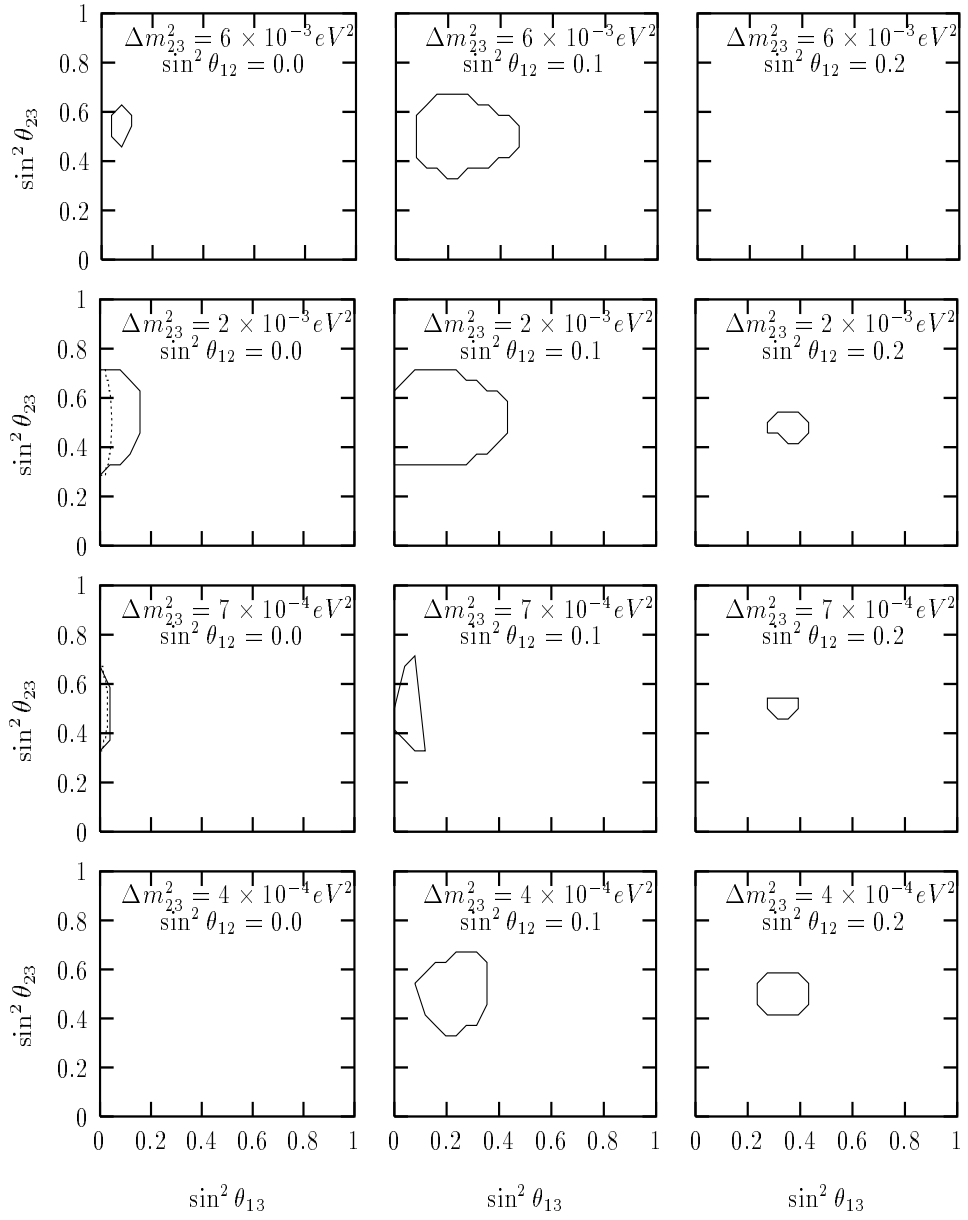


Fig. 4d

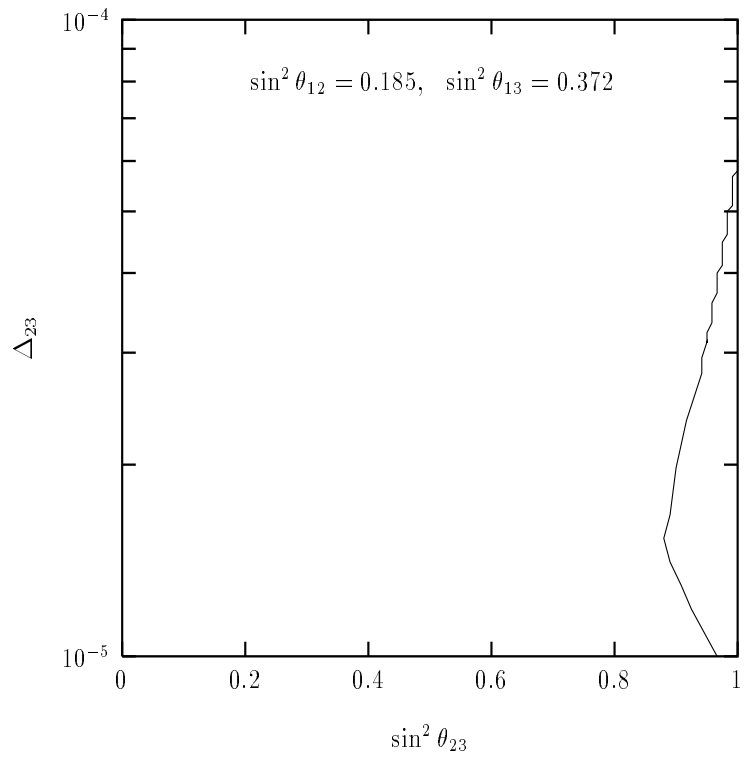


Fig. 4e

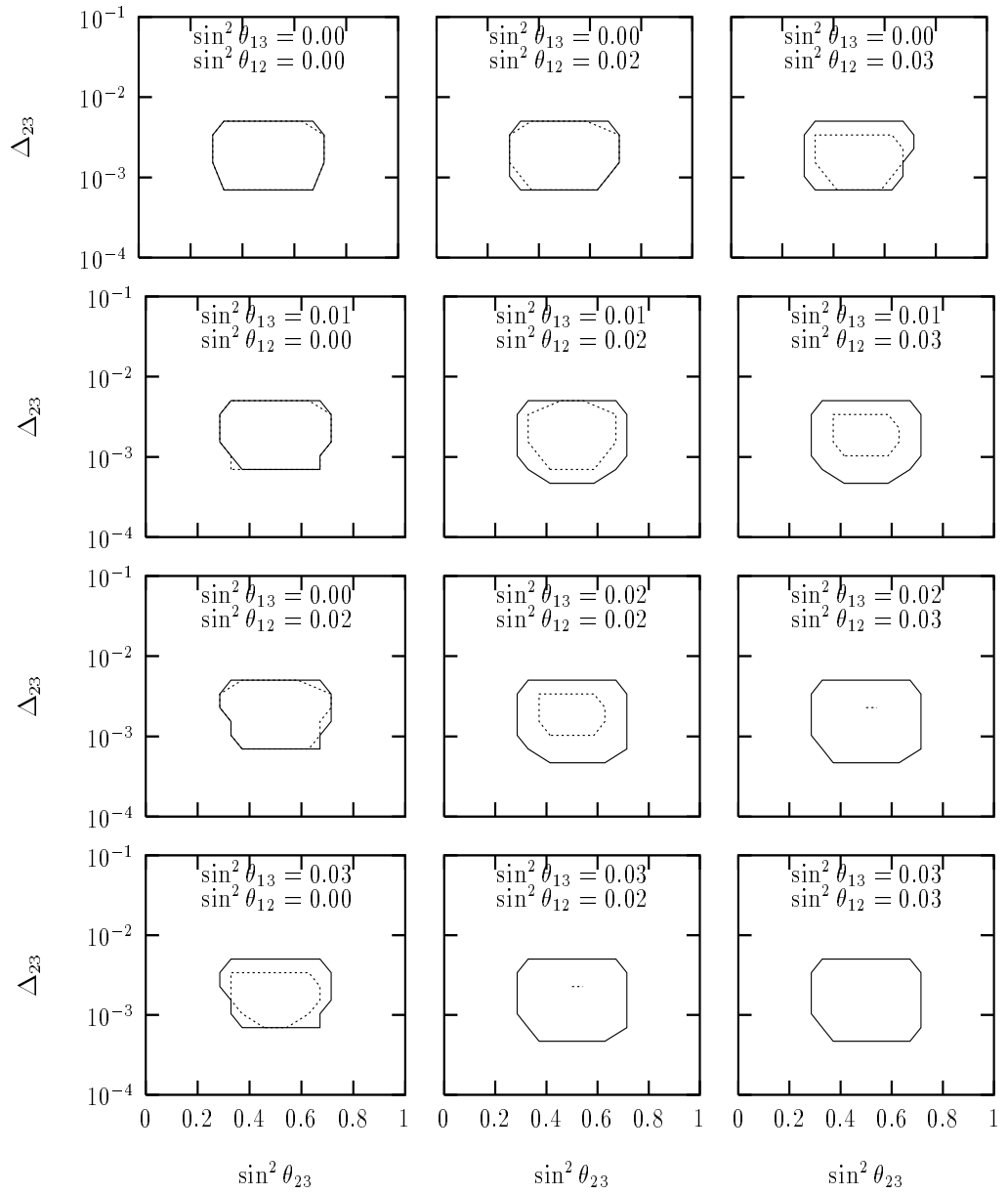


Fig. 5

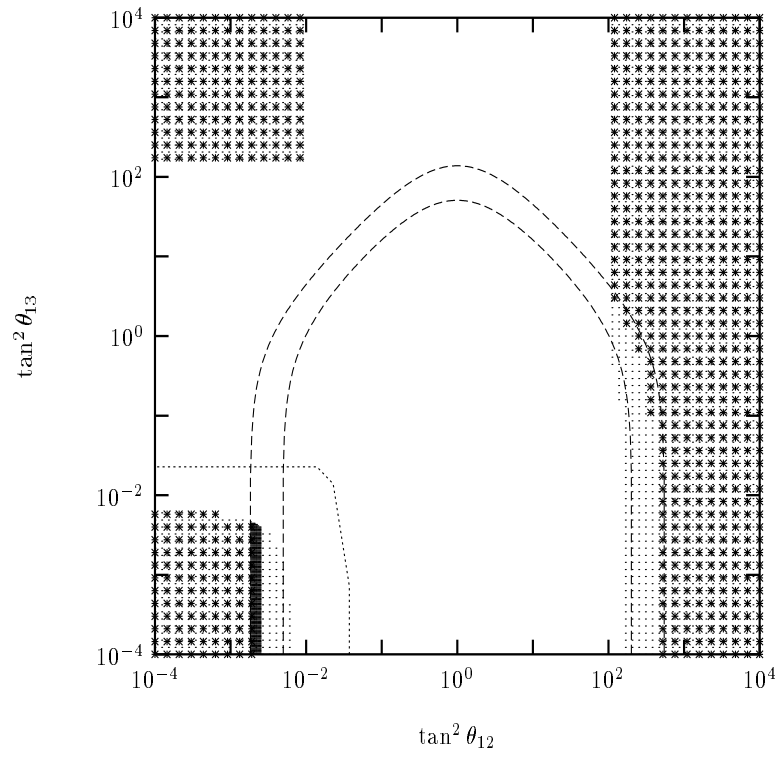


Fig. 6

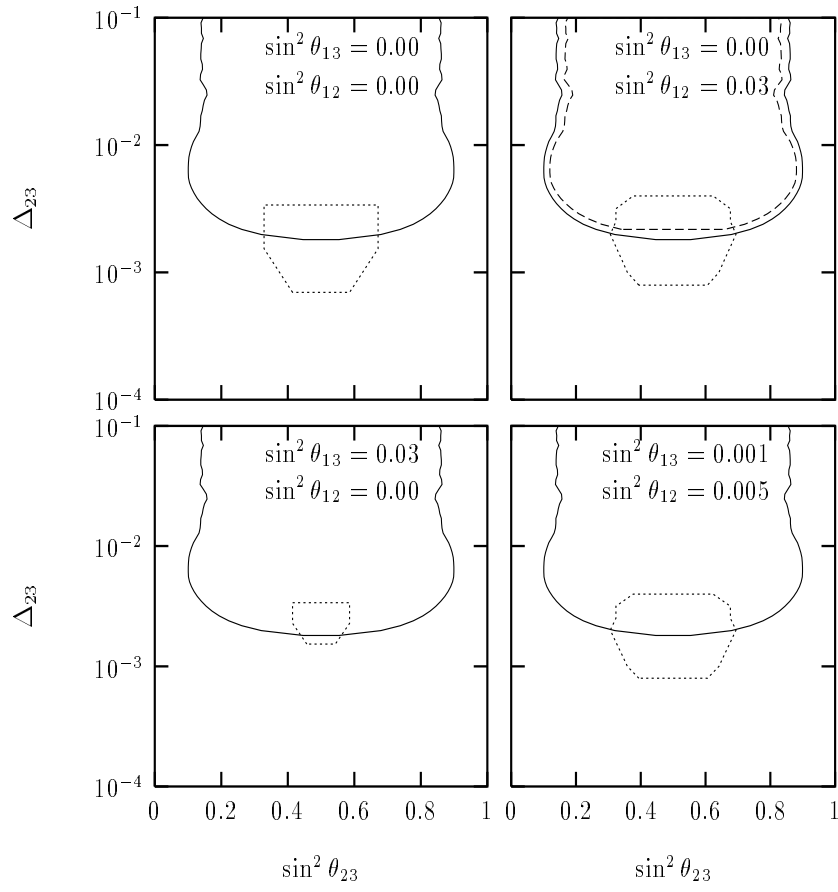


Fig. 7

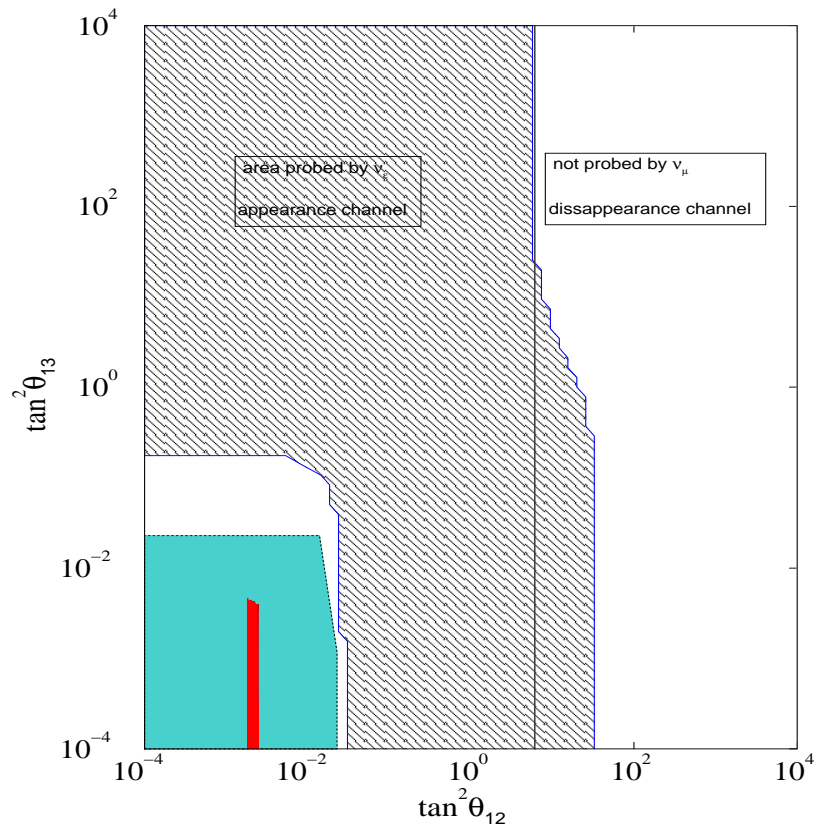


Fig. 8